Investigations of Vanadium Dioxide as a Catalytic Electrode and Support

By

Matthew Curtis Casey

Dissertation

Submitted to the Faculty of the

Graduate School of Vanderbilt University

in partial fulfillment of the requirements

for the degree of

DOCTOR OF PHILOSOPHY

in

Chemistry

December, 2015

Nashville, Tennessee

Approved:

David E. Cliffel, Ph. D.

Sandra J. Rosenthal, Ph. D.

Eva M. Harth, Ph. D.

Richard F. Haglund, Ph. D.

Dedicated to my amazing wife, Amanda. Your radiance grows brighter every day.

A special thanks to my parents, Mike and Janice, who taught me how to respect, love, and especially to learn.

ACKNOWLEDGEMENTS

I have spent more time here than many, and with that comes a great list of people to whom I owe a lot. First and foremost is Dr. David Cliffel, my mentor. I have always been impressed by your wide breadth of knowledge and how you apply that knowledge not only to the myriad of projects going on in your lab but also your numerous collaborations. Your friendliness and approachability has always been appreciated, and the yearly summer party was always one of my favorite social gatherings. Thank you for all your help and patience during my grad school trek.

Dr. Haglund, thank you for giving me an opportunity to collaborate with you for so long. Being regularly exposed to the Physics side of things made sure I was constantly learning new things, and the regular collaboration also greatly helped my professional development, which I am particularly grateful for.

Dr. Rosenthal and Dr. Harth, though I asked both of you to be on my committee when my project was heading in a vastly different direction than it ended up, you have both regularly asked questions that really made me stop and think. Thank you for helping me make it here.

The Cliffel lab has historically been large, but I'll try my best to not forget anyone. To the old building 7 crew – Dr. Kellen Harkness, Dr. Carrie Simpson, and especially Dr. Brian Turner – I am grateful not only for your mentorship in the lab, which helped me a great deal starting out, but also for your inquisitiveness that showed me science is just as much about thinking as it is running experiments. To Dr. Jennifer McKenzie and Dr. Danielle "Watkins" Kimmel, the grad-students-turned-post-docs, thanks for being great

sources of both encouragement and commiseration at times. Lots of both were needed, and you helped more than you know. To my fellow isolationists – Aaron, Adam, and Dave – thanks for being there to chat, discuss (mostly science), and occasionally get distracted by the internet. Having to share hoods and bench space wasn't always easy, but thankfully Adam doesn't take up a lot of space anyway. To the rest of the Cliffel Lab – those past and present – thanks for being the best group anyone could ask for. Having a group that regularly got out of the lab together, even if just for group lunch, was really great.

Dave, Jeremy, Bobby, and Alex, thanks for digging in to the world of board games with me. It's been a fantastic hobby that has been a great source of entertainment and friendship. Y'all have been great.

To the rest of my friends and family all over the place: your constant support, camaraderie, and love is felt and appreciated every day.

And finally, to my wife – without you, I never would have made it here. You are my best friend, my companion, and my rock. Thank you for always being there for me.

TABLE OF CONTENTS

LIST OF TABLES

LIST OF FIGURES

CHAPTER I

INTRODUCTION: VANADIUM DIOXIDE AND THE SEMICONDUCTOR-METAL TRANSITION

In 1959, a "metal-to-insulator" transition was described in certain oxides of vanadium and titanium by Morin.[1] Of the vanadium oxides, VO_2 sparked particular interest due to its transition occurring at 68 °C. This reversible phase transition causes a number of changes in the properties of this material which can be harnessed for a variety of applications. One of these changes is in the reflectivity and optical transmittance of the material; when heated above the transition temperature, the reflectivity and opacity of VO_2 increase, particularly in the near-IR region. This thermochromic response has been tapped in the use of so-called "smart windows", which are designed to naturally darken and reflect some sunlight above a specified temperature.[2] The phase transition in VO_2 is also accompanied by a change in its resistivity by as much as five orders of magnitude, going from a semiconducting state below the transition temperature to a metallic state above.[3] Both of these characteristics also make VO_2 an interesting potential sensor. Theoretical calculations suggest that a catalytic event occurring at the surface of the VO_2 could generate enough energy to induce the phase transition.[4] Therefore, the focus of this dissertation was to determine vanadium dioxide's potential use in catalytic reactions that had not yet been studied with this material, with the long term goal of adapting one or more VO_2-based materials as thermochromic or electrical sensors.

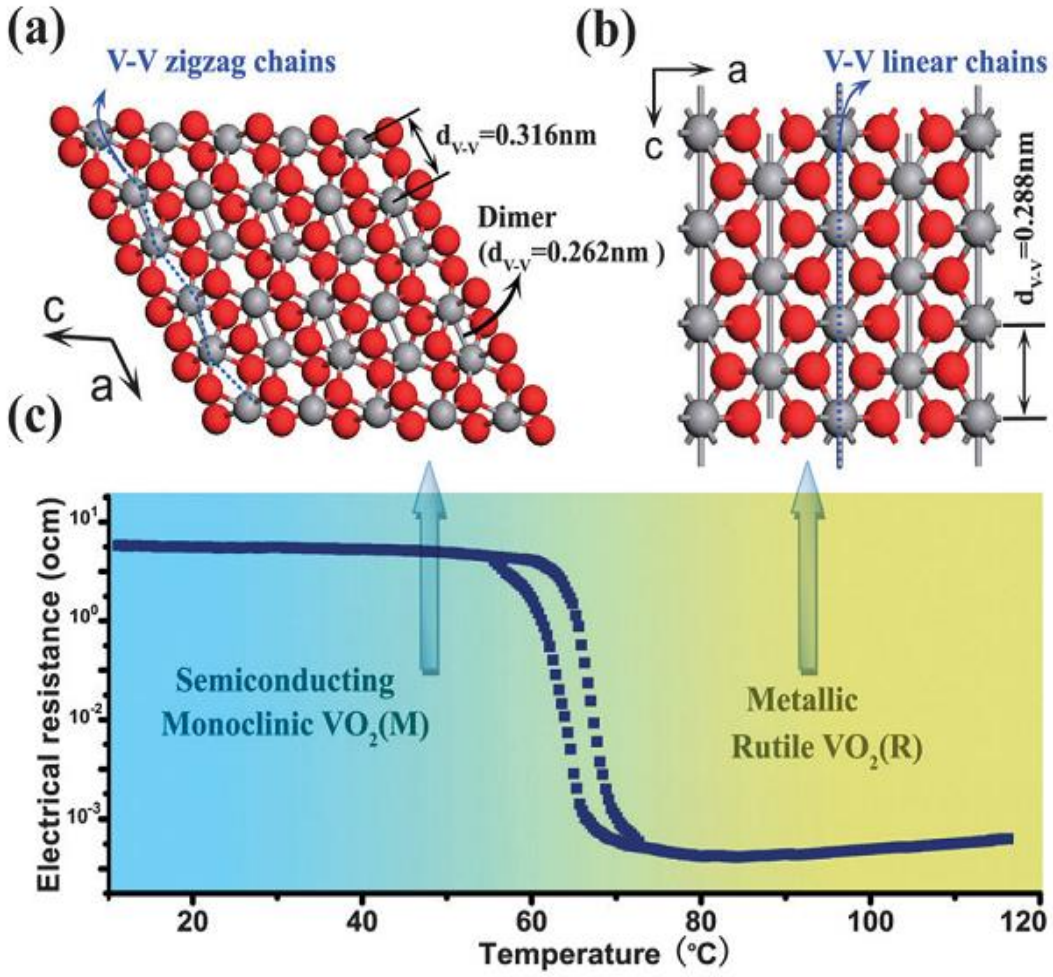

Figure 1. Structure of the (a) semiconducting monoclinic and (b) metallic rutile phases of VO_2, demonstrating the shift in vanadium atoms leading to (c) the large change in resistivity of the material.[5]

Phase Transition in Vanadium Dioxide

Above its phase transition temperature of 68 °C, vanadium dioxide has a metallic character with a rutile lattice structure. In this phase, the vanadium atoms form linear chains in which the average V-V distance is 0.288 nm, which is short enough to allow for overlapping of the d-orbitals and therefore clear paths for electrons to flow.[5] Upon cooling below the phase transition temperature, the vanadium atoms shift from their linear chain formation into V-V dimers as part of a monoclinic structure. While these dimers have an internal V-V distance of only 0.262 nm, each dimer is separated by 0.316 nm, which localizes the d-orbital overlap to individual dimers and leads to increased resistivity in the material by up to five orders of magnitude, as illustrated in Figure 1.[5]

Synthesis and Characterization of Vanadium Dioxide Films and Nanoparticles

Over the last decade, thin films and nanoparticles of VO_2 have been the focus of research aiming for real world applicability (*e.g.* smart windows)[2] due to their greater stability as well as the ability to more easily tune their properties through doping.[3] Chemical vapor deposition (CVD) has been a common technique for the deposition of thin films of many materials for decades, and was first used for VO_2 in the late 1960s.[6] Similarly, physical vapor deposition (PVD) techniques have also been used, most notably sputtering and pulsed laser deposition (PLD).[7,8] Formation of films via sol-gel techniques can be used as a low-cost method that also allows for easier control of doping.[9] Recently, electron beam evaporation has also been used as another low-cost alternative that is more versatile than sol-gel chemistry and uses cheaper materials than the vapor deposition processes.[10] It is also possible to synthesize nanoparticles of VO_2, which exhibit unique

size-dependent properties compared to thin films and bulk VO_2 (*e.g.* larger hysteresis). Growth of nanoparticles on substrates is possible using the same physical deposition techniques previously described, such as PLD.[11] However, more recent studies have demonstrated wet chemical methods to synthesize powders of micro- and nanocrystals of VO_2 via hydrothermal routes.[12–14]

Characterization of VO_2 materials is typically independent of the synthetic method used. X-ray diffraction (XRD) is used to confirm the lattice structure of the material, as shown in Figure 2.[12] Microscopy techniques such as scanning electron microscopy (SEM), transmission electron microscopy (TEM), and atomic force microscopy (AFM) give structural information such as morphology and film thickness. Finally, characterization of the phase transition itself can be done by measuring the reflectivity and resistivity of the sample, as shown in Figure 3.[3] Resistivity measurements are most accurately done using a four-point probe technique originally described by van der Pauw.[15,16] This method measures the voltage between two probes with current flowing between the other two, then repeats this measurement for various combinations of the four probes and averages them, allowing for more precise resistance measurements compared to traditional conductivity probes.

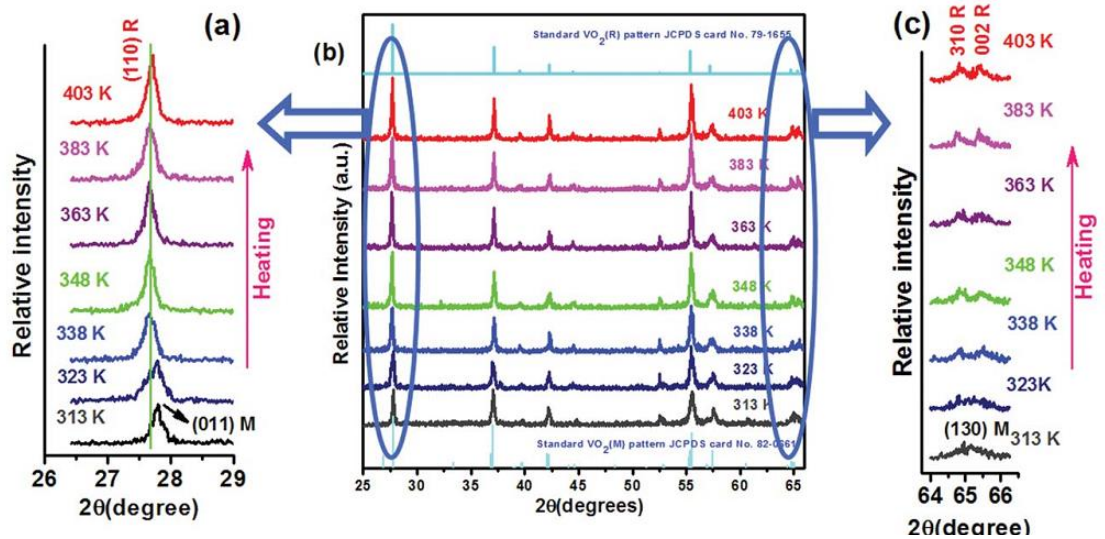

Figure 2. XRD pattern of VO_2 at increasing temperatures, including both the monoclinic (bottom) and rutile (top) patterns.[12]

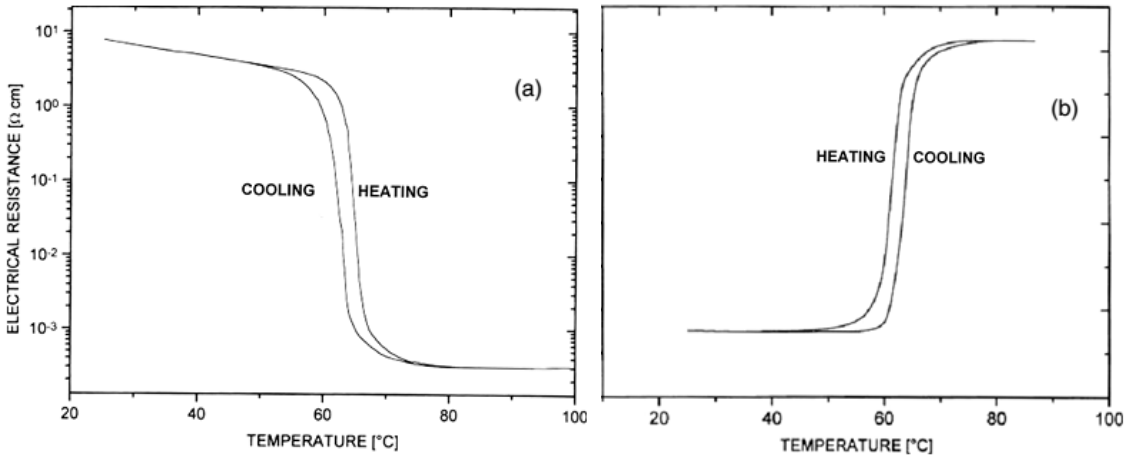

Figure 3. The phase transition in VO_2 is primarily characterized by a sharp change in (a) the resistivity and (b) reflectivity of the material.[3]

Although the innate phase transition of VO_2 occurs at a relatively mild 68 °C, it is advantageous to be able to tailor a given material's transition temperature in order to have a wider applicability. Doping is a common method of tuning the properties of semiconductors, and has also been shown to reliably lower the phase transition temperature of VO_2, particularly when doping with tungsten.[2,3,14,17] A more complicated but effective approach has shown the ability to suppress the transition back the monoclinic phase down to as low as 5 K, though this is well beyond the scope of feasibility for current applications.[18]

Despite the large amount of research that has been focused on this material, the vast majority has been concentrated on its phase transition and related properties, and not the reactions it can participate in. The studies presented in this work aim to bridge this gap and lead towards the eventual development of a thermochromic or electronic chemical sensor.

CHAPTER II*

SURFACE ADSORPTION AND ELECTROCHEMICAL REDUCTION OF TNT ON VANADIUM DIOXIDE

*Portions of this chapter have been published previously: Casey, M. C.; Cliffel, D. E. *Anal. Chem.* **2015**, *87* (1), 334–337.

Background.

2, 4, 6-Trinitrotoluene (TNT) is a well-known explosive compound that is widely used in both military and non-military applications. Field detection of TNT remains an important area of research both for preventative measures as well as decontamination of affected sites.[19,20] Additionally, TNT is a toxic and mutagenic compound that is known to contaminate soil and groundwater – the US Army has estimated that at one point over 1.2 million tons of soil have been contaminated with explosives[21] - increasing the need for sensitive and rapid detection methods.[22–28] Recently, electrochemical methods have been widely used for the detection of TNT due to the inherent selectivity, ease of use, low cost, short analysis time, and low limits of detection.[19,29]

The electrochemical reduction of TNT in water has been shown to occur in three separate, six-electron steps, corresponding to the successive reduction of each of the three nitro groups on the molecule to a hydroxylamine followed by further reduction to an amine group (Figure 4).[30] Typically cyclic voltammetry (CV), linear sweep voltammetry (LSV),

or square-wave voltammetry (SWV) methods are used for TNT detection in water, which show three reductive peaks in the range of -0.4 V to -0.9 V, each corresponding to the complete reduction of one nitro group.[24,25,31]

Various electrodes have been employed in previous studies for TNT reduction. Common materials include glassy carbon[26,27,32–34] or gold[35–37] electrodes, nanoparticle- and nanotube-based electrodes,[32,33,38–40] as well as several metal-oxide based electrodes.[33,38,40] There remains a need, however, for electrode materials with unique properties that provide enhanced sensitivity and wider real world applicability. Various materials have been investigated in this direction, such as the use of nanoporous organosilicas[41] and interdigitated array electrodes (IDAs)[42] to achieve limits of detection of 5 μg L^{-1} and 6 μg L^{-1}, respectively. Of particular note is the use of a TNT immunoassay in conjunction with electrogenerated chemiluminescence (ECL) by Pittman and coworkers to achieve a limit of detection of 0.1 μg L^{-1}.[43] In this work, the viability of vanadium dioxide films as a unique electrode material for the electrochemical reduction of TNT was determined.

The electrochemistry of vanadium (V) oxide has been well studied previously in the realms of sol-gel formation and lithium insertion.[44–49] Vanadium (IV) oxide (vanadium dioxide, VO_2) has received comparatively little attention in the electrochemical sector; however, as discussed in the introductory chapter, it has received considerable interest in the materials science, electrical engineering, and physics communities due to its interesting optical and electronic properties.[18,50–56] At relatively mild temperatures (~340 K), VO_2 undergoes a phase transition from a monoclinic to a rutile lattice structure under heating, which induces a change in its resistance as well as the transmission of light through the material, and can be controlled through doping.[51] In this study, this material was used to

achieve electrochemical detection of TNT as low as 1 μg/L. This compares favorably with previous work in the field, which will be discussed later.[24,32]

Methods.

The deposition of VO_2 films by electron beam evaporation has been described elsewhere.[10] For this work, films were deposited on indium tin oxide (ITO)-covered glass slides (Corning®, Boro-Aluminosilicate 25x25x0.7 mm). A 0.5 cm portion of the slide was masked during deposition so an electrical connection could be made to the potentiostat via the ITO. Electrochemical measurements were performed using a CH Instruments (Austin, TX) 660A electrochemical workstation. The VO_2 working electrode area was 1.767 cm^2. Ag/AgCl (3 M KCl) was used as the reference electrode, and a platinum mesh was employed as the counter electrode. The electrolyte solution consisted of 0.1 M KCl in water adjusted to pH 9 using NaOH. A rubber septum was used to seal the vessel and the system was purged with high-purity nitrogen for a minimum of 30 minutes prior to each experiment. Reference and counter electrodes were inserted through the septum prior to purging. Linear sweep voltammetry experiments were performed by scanning from 0 to -1 V at a scan rate of 10 mV s^{-1}. TNT was purchased from Cerilliant (Round Rock, TX) as 1000 ppm standards in acetonitrile. Aliquots of TNT were added via a syringe to achieve concentration ranges between 1 μg L^{-1} and 25 mg L^{-1}, and voltammograms were recorded after stirring for 10 minutes following each addition. In adsorptive stripping experiments, the working electrode was held at a fixed potential of 0.0 V during stirring. Stirring was not performed during the scans.

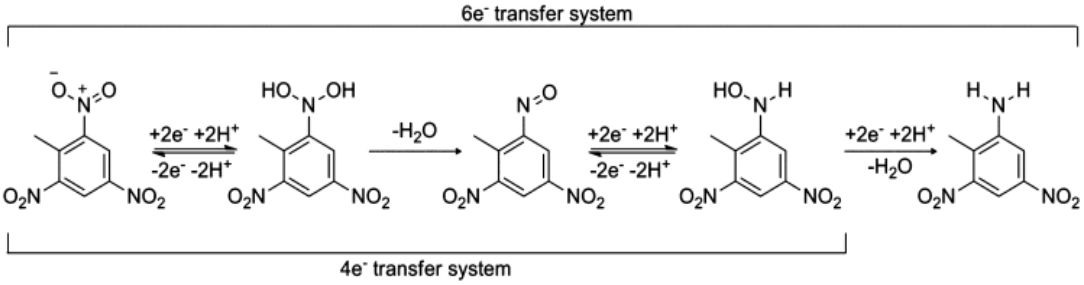

Figure 4. Electrochemical reduction of one nitro group of TNT.[30]

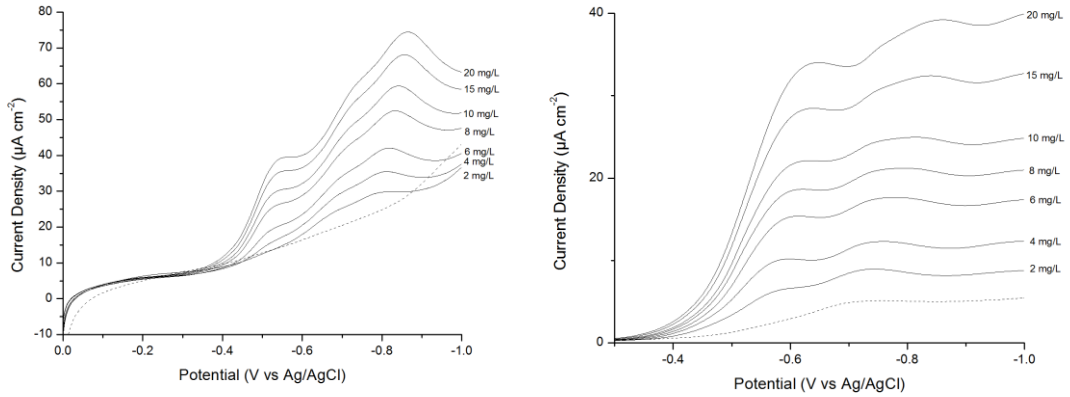

Figure 5. Linear sweep voltammogram of TNT reduction on (left) a VO_2 film and (right) a bare ITO film. Reduction potentials for the VO_2 film at 20 mg L^{-1} were -0.542 V, -0.732 V, and -0.861 V vs Ag/AgCl, and -0.630 V and -0.839 V vs Ag/AgCl for the ITO. Dotted line represents the background scan in the basic electrolyte in the absence of TNT.

Results and Discussion.

To determine the reduction potentials of TNT on vanadium oxide films, linear sweep voltammetry was performed. Three reduction peaks were observed above 1 mg/L, which is consistent with previous electrochemical reduction studies.[27,38,40] These peaks had potentials of -0.542 V, -0.732 V, and -0.861 V vs Ag/AgCl at 20 mg/L, as seen in Figure 5, and notably shift towards more negative potentials as TNT concentration increases. Additionally, the observed reduction peaks exhibit a broadness that is characteristic of a kinetically limited reduction process. This process is chemically irreversible, as has been observed previously.[24,39]

Control experiments were performed to determine the effect of the substrate on the observed activity by examining the ability of ITO on glass to electrochemically reduce TNT. Similar reduction behavior to that of the VO_2 films was observed with this material, as shown in Figure 5. Broad, negatively shifting reduction peaks were again observed; however, only two reduction peaks are seen, with peaks having reduction potentials of -0.630 V and -0.839 V vs Ag/AgCl at 20 mg L^{-1}. Furthermore, these peaks are less defined than what is seen with VO_2 films.

In order to test the sensitivity of VO_2 films for TNT reduction, adsorptive stripping voltammetry was utilized. This preconcentration technique has been used previously in trace analysis due to its higher sensitivity and lower limits of detection,[57] and was successfully employed by Wang *et al* for TNT reduction on modified glassy carbon electrodes.[32] Figure 6 shows stripping voltammograms for TNT reduction on a VO_2 film at concentrations from 1-5 μg L^{-1}. Remarkably, three peaks can be seen even at 1 μg L^{-1}, with potentials of -0.564 V, -0.626 V, and -0.756 V vs Ag/AgCl. The peak currents for the first

reduction peak reveal a linear response to TNT concentration, which is in strong agreement with what has been observed previously.[24,25,32,33,37] Concentrations from 100-1000 μg L^{-1} were also measured and demonstrate a linear response, as shown in Figure 7.

Based on these results, it is likely that surface adsorption of TNT is the primary mechanism for these films, similar to other systems such as nanoparticle- and nanotube-modified electrodes.[32,33,39] In order to confirm this, the dependence of the peak current on scan rate (υ) was measured, as shown in Figure 8. At low concentrations of TNT, peak current increases linearly with $\upsilon^{1/2}$. At higher concentrations, a linear correlation is also seen, though to a lesser degree. However, due to the difficulty in resolving peaks at fast scan rates, particularly at high concentrations, a more thorough study may be necessary to fully elucidate this process.

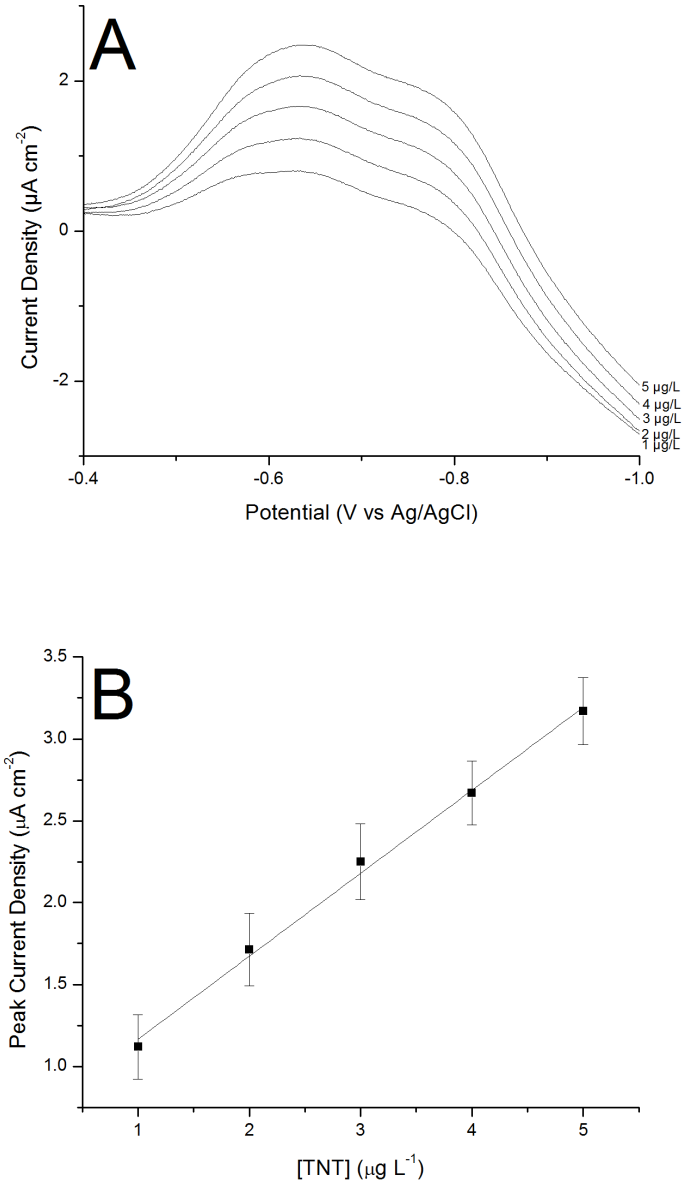

Figure 6. (A) Background-subtracted stripping voltammogram of TNT reduction on a VO_2 film after 600 s accumulation. Concentrations of TNT used were (from bottom to top) 1-5 µg L^{-1}, respectively. Reduction potentials at 1 µg L^{-1} were -0.564 V, -0.626 V, and -0.756 V vs Ag/AgCl. (B) Calibration curve for the first reduction peak, demonstrating a linear current response to TNT concentration.

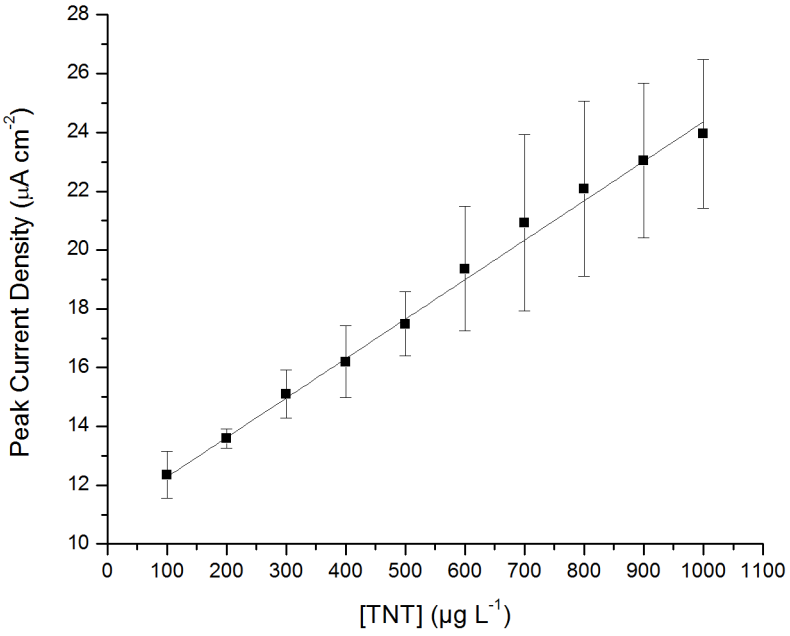

Figure 7. Current density of first reduction peak in the range 100-1000 μg L^{-1}.

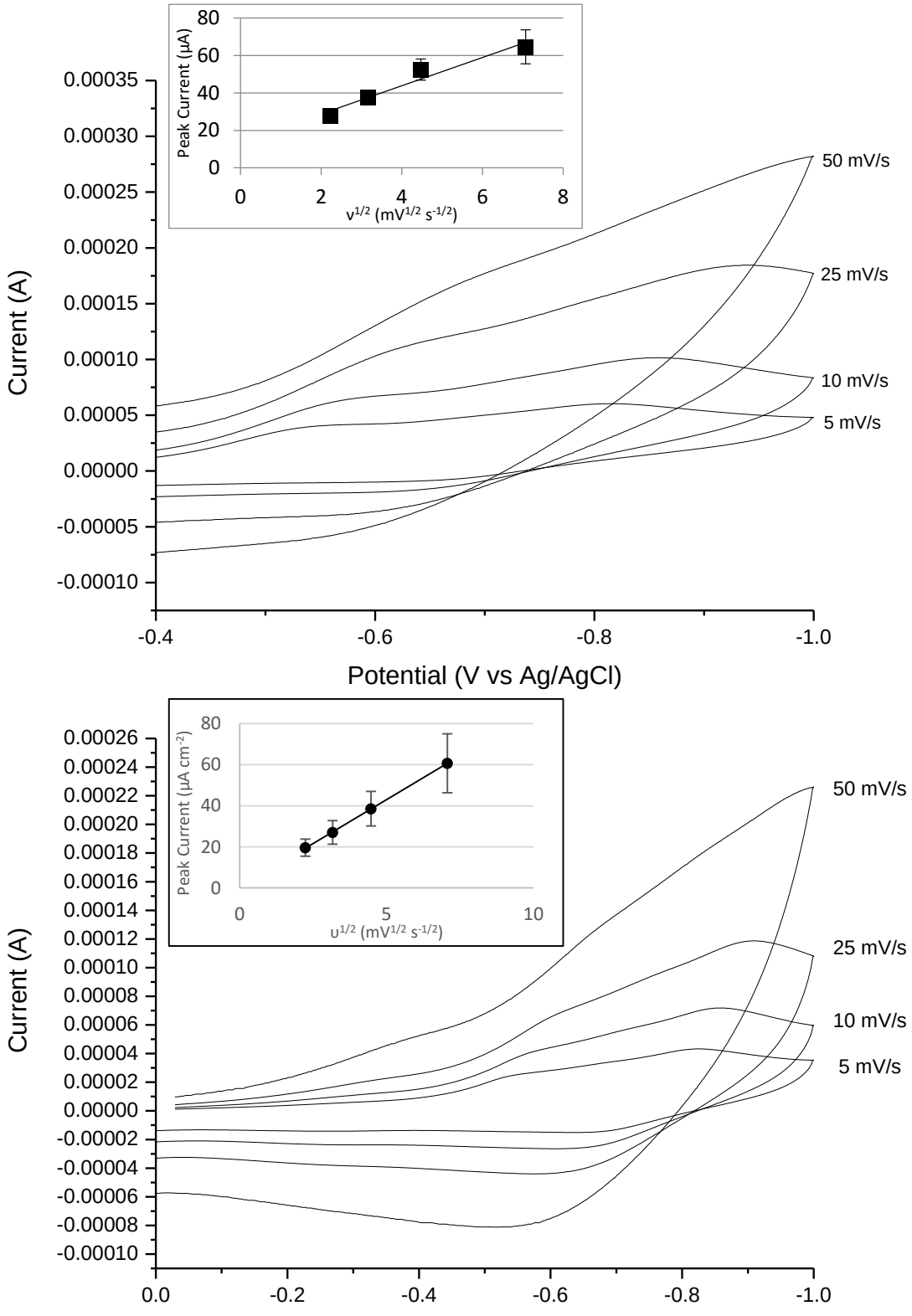

Figure 8. TNT reduction on VO_2 at various scan rates for (top) 5 mg L^{-1} and (bottom) 5 μg L^{-1}. Insets show linear fits for peak current vs $\upsilon^{1/2}$.

Conclusions and Future Work.

The work presented here provides the first evidence that VO_2 can be used for the electrochemical reduction of TNT. Three reduction peaks were observed in the potential range -0.50 to -0.90 V vs Ag/AgCl, which is consistent with previous work. The potential of the three peaks was dependent on TNT concentration, with the peaks shifting towards more negative potentials with increasing concentration. The data suggest a kinetically limited reduction process on these materials. Control experiments using ITO-covered glass showed an even stronger kinetically-limited response. Remarkably, low concentration studies utilizing adsorptive stripping voltammetry showed TNT detection as low as 1 μg L^{-1}, with a linear response to TNT concentration. Due to the likely role of surface adsorption for these materials, efforts have begun to focus on the use of higher surface area VO_2 in the form of micro- and nanoparticles, the syntheses of which will be further discussed in Chapter III.

Acknowledgements.

I would like to thank the laboratory of Dr. Richard Haglund, especially Dr. Jed Ziegler and Robert Marvel, for the preparation of the VO_2 films that were used in this work and their great knowledge of VO_2. I would also like to thank Evan Gizzie, who helped me out a lot at the start of this project and helped get me up to speed with electrochemistry. This work was supported by the Defense Threat Reduction Agency, HDTRA 1-10-1-0047.

CHAPTER III

OXIDATION OF CARBON MONOXIDE ON VANADIUM DIOXIDE-SUPPORTED GOLD CATALYSTS

Background.

Gold was historically considered catalytically inactive until work by Bond *et al.* in 1973 showed that supported gold particles exhibited catalytic activity for olefin hydrogenation.[58,59] Over a decade later, Haruta and coworkers demonstrated in 1987 that gold deposited on oxides of Fe, Co, and Ni showed surprising catalytic activity for the oxidation of CO at relatively mild conditions.[60] Since those pioneering works, a variety of research has used nanoparticulate gold as a primary catalytic center for many different catalysis reactions. When deposited on metal oxide supports (typically first row transition metals), gold has been discovered to catalyze several important industrial oxidation reactions, including the water-gas shift (WGS) reaction and the epoxidation of propene.[61–63] However, the ability of gold nanoparticles to catalyze CO oxidation has been the primary focus of recent literature.[58,64–68] Traditionally, heterogeneous gold catalysts like the ones mentioned above are supported by a metal oxide which stabilizes the gold species and may also participate in the catalytic reaction.[69] In the case of carbon monoxide oxidation, the catalytic site is found at the interface between the gold particle and the metal oxide, as demonstrated in Figure 9.[66] Because of this, smaller gold particles which have a higher ratio of interfacial and low-coordination gold sites show higher activity for CO oxidation.[69]

Most common supports are oxides of the first row of transition metals, such as Ti, Mn, and Fe.[61,70–72] Table 1 summarizes some of the work performed in the last two decades using metal oxide-supported gold CO oxidation catalysts. There are several possible methods for synthesizing and depositing small gold particles onto these supports. Co-sputtering and gas-phase grafting evaporate gold precursors to deposit gold onto the surface from the gas phase.[73,74] In impregnation, auric acid is added to the stirring support, then evaporated and calcined in air.[75] Unfortunately, this method typically produces gold particles larger than 30 nm, owing to weak interaction with the support as well as residual chlorides promoting coagulation.[68] In coprecipitation, the support is dissolved in a solution to which the gold acid is added, followed by precipitation of the supported gold catalyst from the solution.[76] Deposition-precipitation (DP) uses a pH-adjusted $HAuCl_4$ solution added to the stirring support to deposit small gold particles on the surface of the support, usually in the 2-10 nm range.[68,77] Additionally, gold nanoparticles in the form of monolayer-protected clusters (MPCs) can be deposited on supports via impregnation and sintered to the supports after thermal treatment.[78–80] This method offers the advantage of allowing for finer control of gold nanoparticle size by synthesizing particles in a separate step from the deposition. Of these various methods, deposition-precipitation and impregnation of MPCs are ideal for their ability to produce small gold particles on TiO_2 for the production of active CO oxidation catalysts.

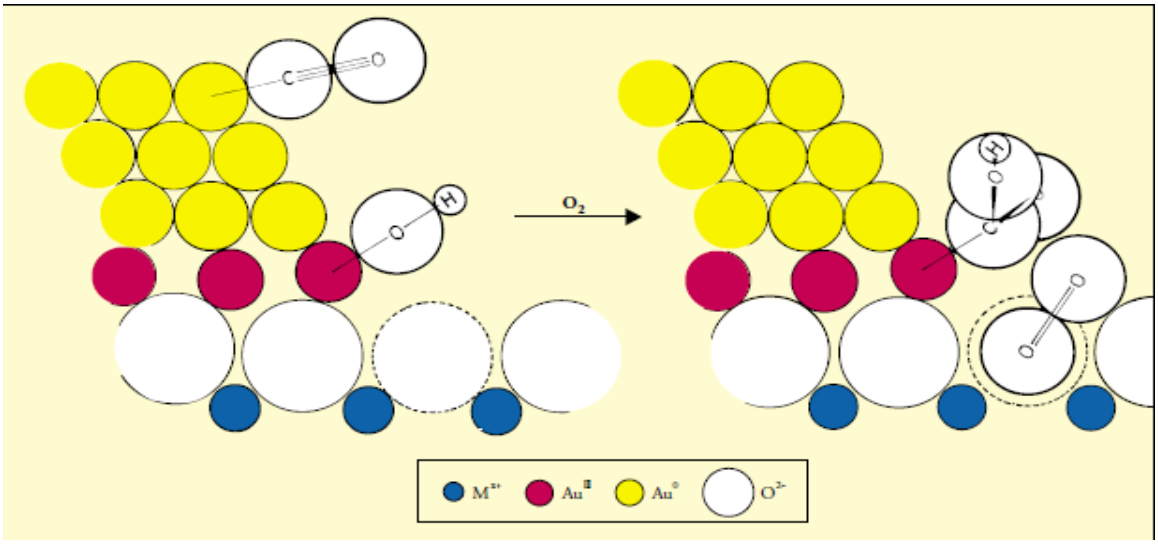

Figure 9. Mechanism of CO oxidation catalysis at the gold-metal oxide interface. A carbon monoxide molecule binds to a low coordination gold atom, while a hydroxyl ion from the support lattice migrates to an interfacial site, leaving an anion vacancy. This vacancy is filled by molecular oxygen as O_2^- while the carbon monoxide and hydroxyl react to form a carboxyl group. The carboxyl is then oxidized by the O_2^-, forming CO_2.[66]

Table 1. Metal oxide supports for gold CO oxidation catalysts

Support	**Preparation Method**
MnO_x[60,61,70]	Coprecipitation
Fe_2O_3[60,71,72,81,82]	Deposition-precipitation, coprecipitation
NiO_x[60,82]	Coprecipitation
CoO_x[82]	Impregnation
Co_3O_4[60]	Coprecipitation
CeO_2[83,84]	Deposition-precipitation, coprecipitation
Al_2O_3[75]	Impregnation
Y_2O_3[85]	Deposition-precipitation
SiO_2[86,87]	Physical vapor deposition
TiO_2[74,77,79,80,88–113]	Deposition-precipitation, vapor deposition, impregnation, coprecipitation, gas-phase grafting

Despite other transition metals being popular avenues of research for CO oxidation, vanadium has received very little attention in the context of this reaction. A report by Zhu *et al.* described theoretical calculations suggesting V_2O_5 nanotubes may be able to catalyze CO oxidation,[114] but experimental data remains surprisingly absent in the literature. The aim of this research is to fill this void by synthesizing a Au/VO_2 catalyst that is active for CO oxidation and may eventually be adapted as a catalytic sensor that also utilizes the unique optical properties of VO_2. Despite the lack of literature concerning Au on VO_2 as a catalytic material, this material should display similar activity for CO oxidation to other metal-oxide based catalysts.

Materials and Methods.

Synthesis of Au/TiO_2 and Au/V_2O_4 catalysts using deposition-precipitation

In order to synthesize active Au/VO_2 catalysts, a procedure for synthesizing Au/TiO_2 CO oxidation catalysts using deposition-precipitation was adapted.[77] The first catalysts synthesized used either TiO_2 (as a control) or V_2O_4. The V_2O_4 used in these experiments is the precursor material used in the deposition of stoichiometric VO_2 films as mentioned in Chapter I.[10] This material was initially chosen as an analog of VO_2 due to the inability to synthesize monoclinic VO_2 at the time. In an example synthesis, 11 mmol TiO_2 (Hombikat® catalyst grade, Sigma-Aldrich) or V_2O_4 (99.5% pure, 100 mesh, Materion) powder was slurried in approximately 75 mL H_2O for 30 minutes. Then, 0.1 M NaOH was added to bring the reaction to pH 8.0, followed by addition of 1.024 mL of 0.1 M $HAuCl_4$ aqueous solution directly to the stirring support. Following addition of the gold aqueous solution, more 0.1 M NaOH was added to maintain a pH of 8.0-8.5. After 2 h, the material

was washed 3x with H_2O, then dried under vacuum in a desiccator overnight. Au/TiO_2 powder dried as light purple chunks (as opposed to the white TiO_2 starting material), which were broken up using a mortar and pestle after drying. Au/V_2O_4 powder saw no color change from the starting black powder. Catalysts were characterized by transmission electron microscopy (TEM) or scanning electron microscopy (SEM) to determine deposited gold nanoparticle size.

Synthesis of Au/TiO_2 Au/V_2O_4, and Au/VO_2 catalysts using monolayer-protected gold nanoparticles

For impregnation of MPCs onto the metal oxide supports, another literature method was adapted.[78,79] Octanethiol-capped gold nanoparticles were first synthesized using the two-phase Brust method.[115] Briefly, 2.18 g tetraoctylammonium bromide (TOAB, 4 mmol) was dissolved in 60 mL toluene and added to approximately 500 mg aqueous gold acid ($HAuCl_4•3H_2O$, 1.27 mmol) in 30 mL H_2O. The reaction was stirred for 1 h to allow transfer of the gold acid to the toluene. Water was then removed using a separatory funnel. The toluene-soluble reaction was transferred to a chilled flask, and approximately 800 µL octanethiol (4.6 mmol) was added. After 1 min, 0.4 g chilled $NaBH_4$ (10.5 mmol) was quickly added to the reaction to reduce the gold and form the MPCs. After 1.5 h, the toluene was removed via rotary evaporation, followed by addition of ~150 mL ethanol to remove unreacted material overnight. MPCs were then washed with acetonitrile and centrifuged. Washing was repeated 5-10 times prior to drying via rotary evaporation. MPCs were characterized using TEM and thermogravimetric analysis (TGA) to determine average particle diameter and composition, respectively.

To deposit MPCs onto the metal oxide supports, ~500 mg of TiO_2 or VO_2 was added to 40 mL DCM and stirred. To this, 5 mg MPCs in DCM were added and stirred for 3 h. As the MPCs adsorb onto the support, color fades from the solution and begins to appear on the support powder. After reaction, the catalysts were transferred to test tubes, washed with DCM, and centrifuged. This was repeated 3 times before being dried in a dessicator under vacuum overnight. The dry powders were placed in ceramic boats and calcined in a tube furnace heated to 300 °C under air flow. This thermal treatment serves both to remove the organic capping ligands from the adsorbed gold nanoparticles as well as to sinter the particles to the metal oxide support. Catalysts were characterized as described above.

Synthesis of Vanadium Dioxide Nanoparticles

Recently, synthetic routes to micro- and nanoparticles of VO_2 have been described.[12–14] These methods were adapted and are currently being used in the Cliffel laboratory to synthesize "nano-asterisks" of VO_2, and preliminary experiments have been performed to use these as supports for CO oxidation as has been described in the rest of this chapter. To synthesize these VO_2 nanoparticles, a slurry of 450 mg V_2O_5 (Aldrich) in H_2O was heated to 90 °C in a water bath. To this, 1.500 mL H_2SO_4 was added, followed by swift addition of 500 µL hydrazine monohydrate, leading to a blue solution of the vanadyl ion, VO^{2+}. 1 M NaOH was then added until the solution reached a pH of 4.0 and allowed to stir for 15 minutes before cooling to room temperature. The product was vacuum filtered, washed with H_2O, then transferred to a Teflon™ cup and placed in a stainless steel autoclave. This vessel was placed in a muffle furnace and kept at 230 °C for 48 h. The resulting product was filtered and washed again with H_2O and dried in an oven overnight.

Deposition of AuNPs onto these materials was done via impregnation of hexanethiol-capped MPCs as described above.

Catalytic measurements of Au/TiO_2 and Au/V_2O_4 for the oxidation of CO

Catalyst activities for CO oxidation were measured in a fixed bed reactor coupled to a gas chromatograph (GC) equipped with a thermal conductivity detector. In order to detect CO_2 production, the GC was equipped with a second column that selectively separated the CO_2 so that it could be distinguished from the air peak. The first column is a Porapak Q column, which separates the CO_2. The second column, a molecular sieve column, then separates the air (where normally the CO_2 peak would be hidden) and CO peaks. In a typical experiment, ~200 mg of catalyst was packed into the stainless steel bed which was then surrounded by a furnace and a steady flow of 1% CO in air (A-L Compressed Gases) at a typical flow rate of ~5 mL/min was flowed through the system. The system was allowed to equilibrate for 15-20 mins at room temperature and after each temperature increase before taking measurements. To determine the amount of CO oxidation, the ratio of peak areas CO_2:CO was used. As suggested by Li and coworkers,[77] $T_{50\%}$ (defined as the temperature at which 50% conversion is observed) was calculated for each catalyst and used as a basis for comparison for the different catalysts.

Results and Discussion.

Synthesis of Au/TiO_2 and Au/VO_2 catalysts using deposition-precipitation

A typical Au/TiO_2 catalyst synthesized using the DP method produced Au nanoparticles (AuNPs) having an average diameter of 8.0 nm supported on the TiO_2 surface

(Figure 10). Au/V_2O_4 catalysts produced using the same procedure had much larger particles of 34 ± 7 nm as determined by SEM (Figure 11).

Synthesis of Au/TiO_2 and Au/VO_2 catalysts using monolayer-protected gold nanoparticles

Catalysts prepared using impregnation of MPCs used octanethiol-capped gold nanoparticles of average diameter 2.3±0.6 nm. After deposition on the TiO_2 support and subsequent thermal treatment, gold nanoparticles of size 3.4±0.9 nm were found to be deposited on the support (Figure 12). The increase in size and polydispersity compared to the precursor nanoparticles are likely due to agglomeration of some particles, which has been demonstrated previously.[79]

In order to synthesize Au/V_2O_4 catalysts, hexanethiol-capped gold nanoparticles of average diameter 2.1±0.5 nm were deposited on V_2O_4 and treated under similar conditions as the Au/TiO_2 catalysts.

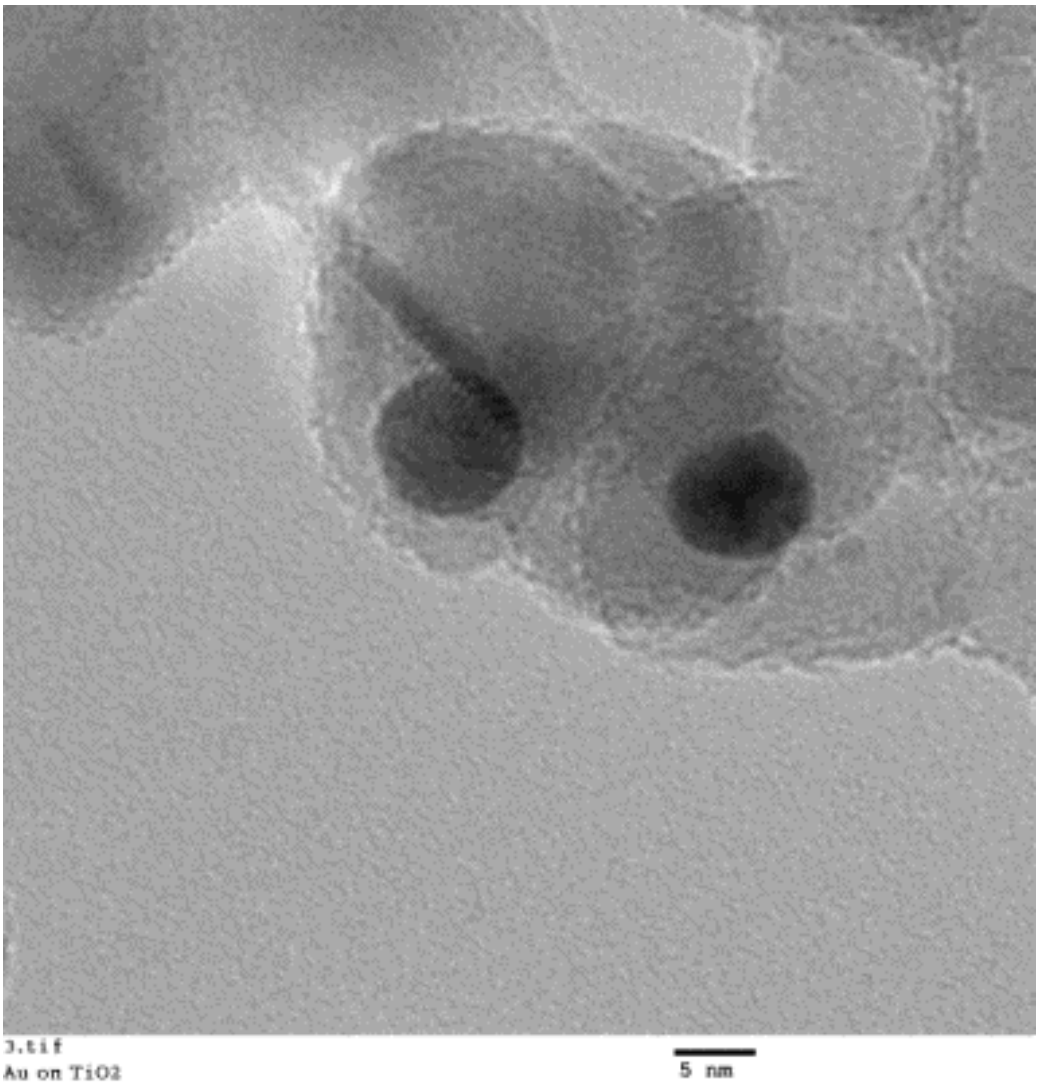

Figure 10. TEM image of Au nanoparticles deposited on TiO_2. Scale bar is 5 nm.

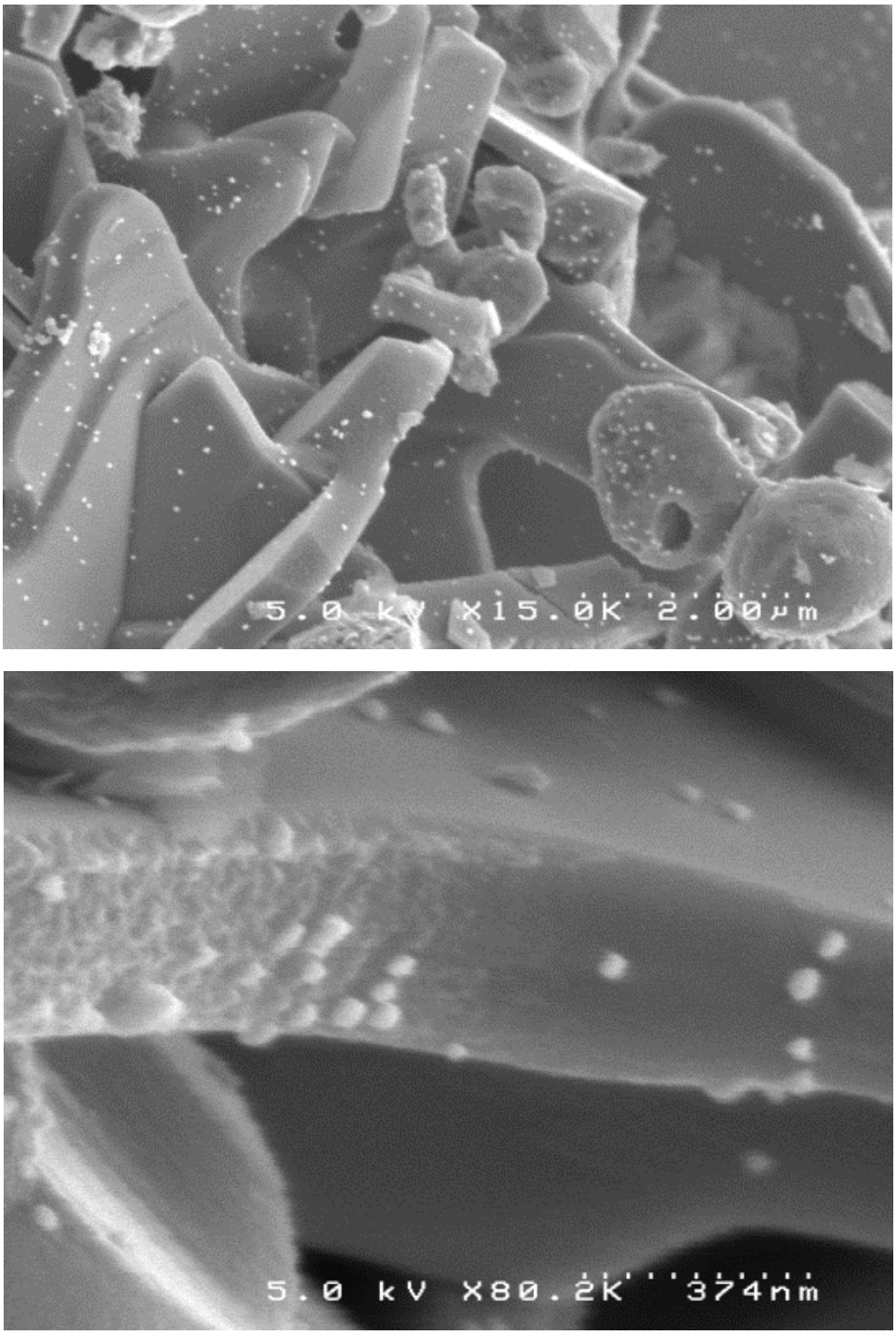

Figure 11. SEM images of Au nanoparticles deposited on VO_2. Average diameter 34±7nm. a) Scale bar is 2.00 µm. b) Scale bar is 374 nm.

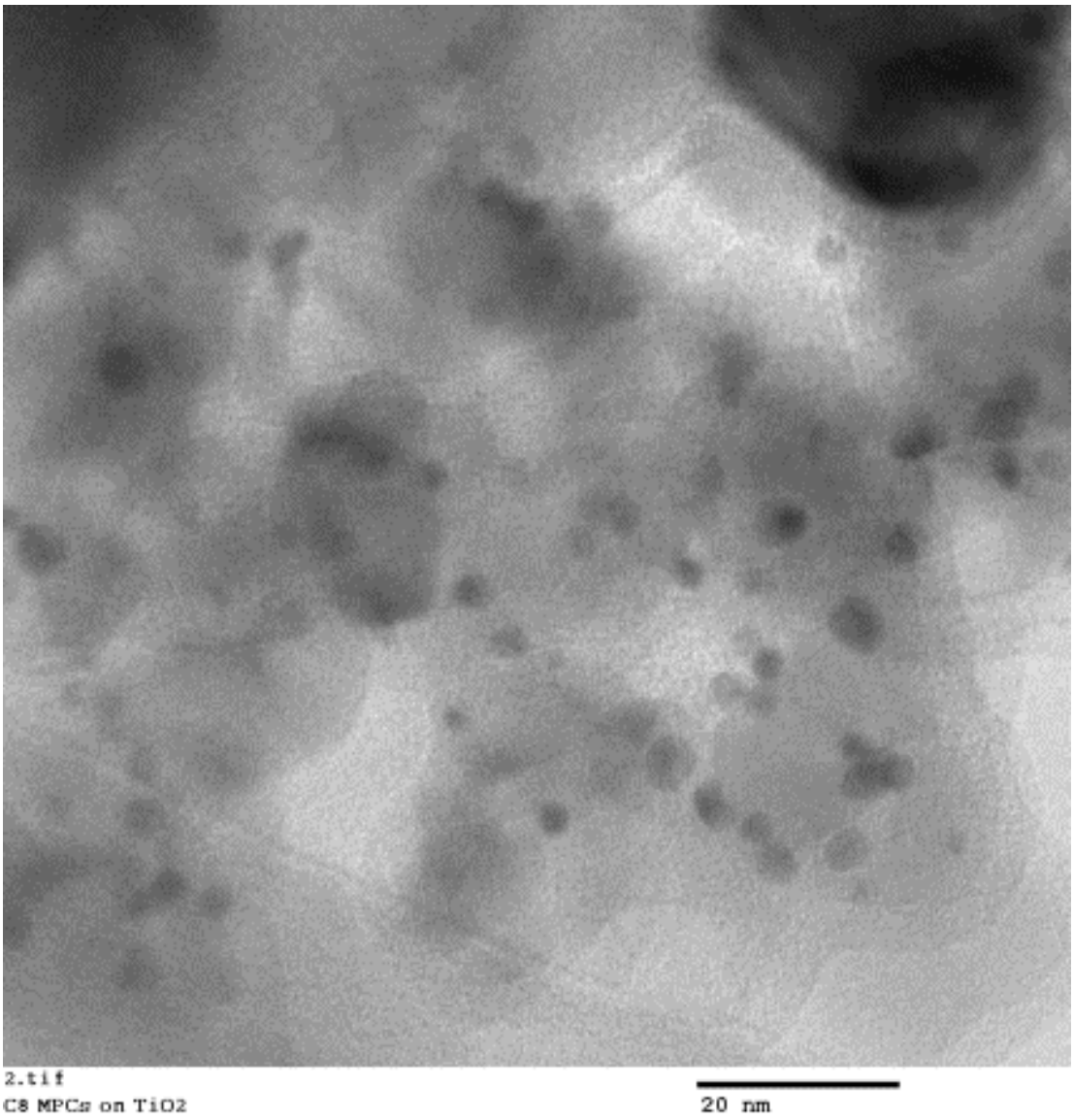

Figure 12. Au nanoparticles deposited on TiO_2 using monolayer-protected gold nanoparticles. Scale bar is 20 nm.

Catalytic activity of Au/TiO_2 and Au/V_2O_4 catalysts prepared by deposition-precipitation

To determine the activity of each catalyst for the oxidation of CO, the ratio of peak areas (CO_2:CO) was used. A sample chromatogram is shown in Figure 13, demonstrating how use of a CO_2-selective column allows for clear determination of the peaks of interest. Figure 14 shows the activity of the Au/TiO_2 and Au/V_2O_4 catalysts prepared via deposition-precipitation as a function of temperature. $T_{50\%}$ for Au/TiO_2 was found to be 55 °C, while $T_{50\%}$ for Au/V_2O_4 was 106 °C. The activity of the Au/TiO_2 catalyst for this reaction was much lower than that of Li *et al.*'s catalysts, which were reported to have $T_{50\%}$ values near 20 °C.[77] This difference in activity is likely due to differences in gold particle sizes on the catalyst, since smaller gold particles (< 5 nm) are known to be the most active for CO oxidation.[58,66,68] This is also a likely explanation as to why the Au/V_2O_4 catalysts, which showed gold particle sizes of 34 ± 7 nm, showed even less activity for CO oxidation. Although these results are not as impressive as established catalyst materials, the ability of these Au/V_2O_4 catalysts to promote CO oxidation (albeit at higher temperatures than other supports) was established for the first time.

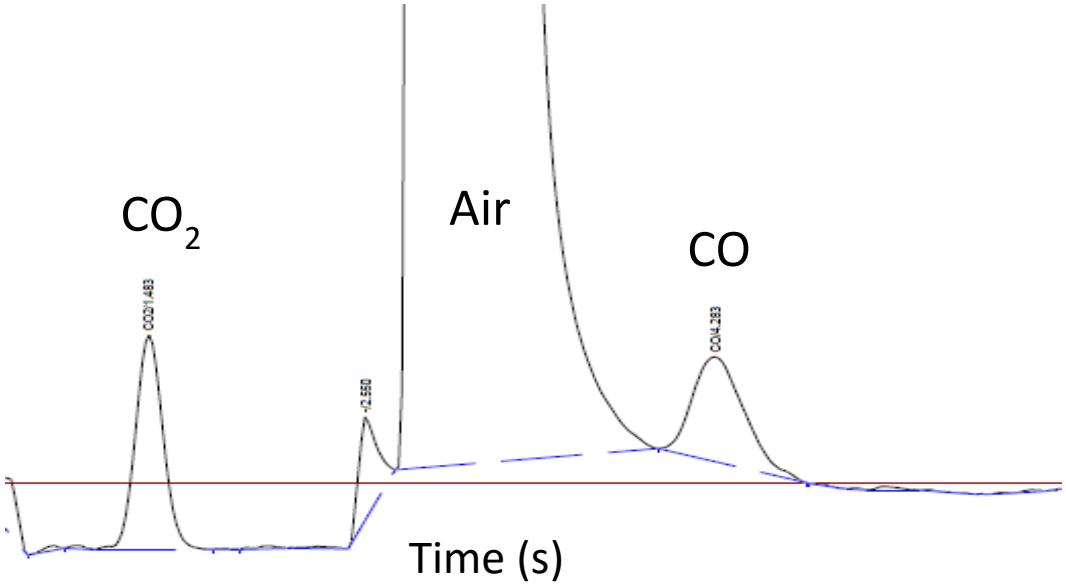

Figure 13. Sample chromatogram showing CO_2 (left), Air (middle), and CO peaks. To calculate CO_2:CO, the ratio of the areas of the peaks is used.

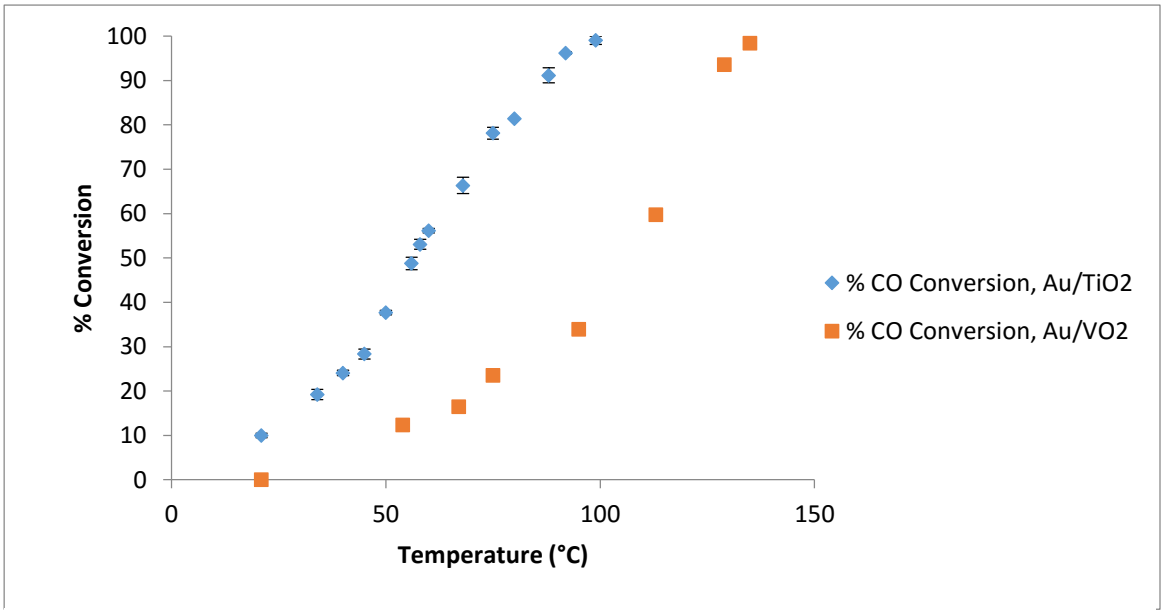

Figure 14. Catalytic activity of Au/TiO_2 and Au/V_2O_4 catalysts prepared via deposition-precipitation

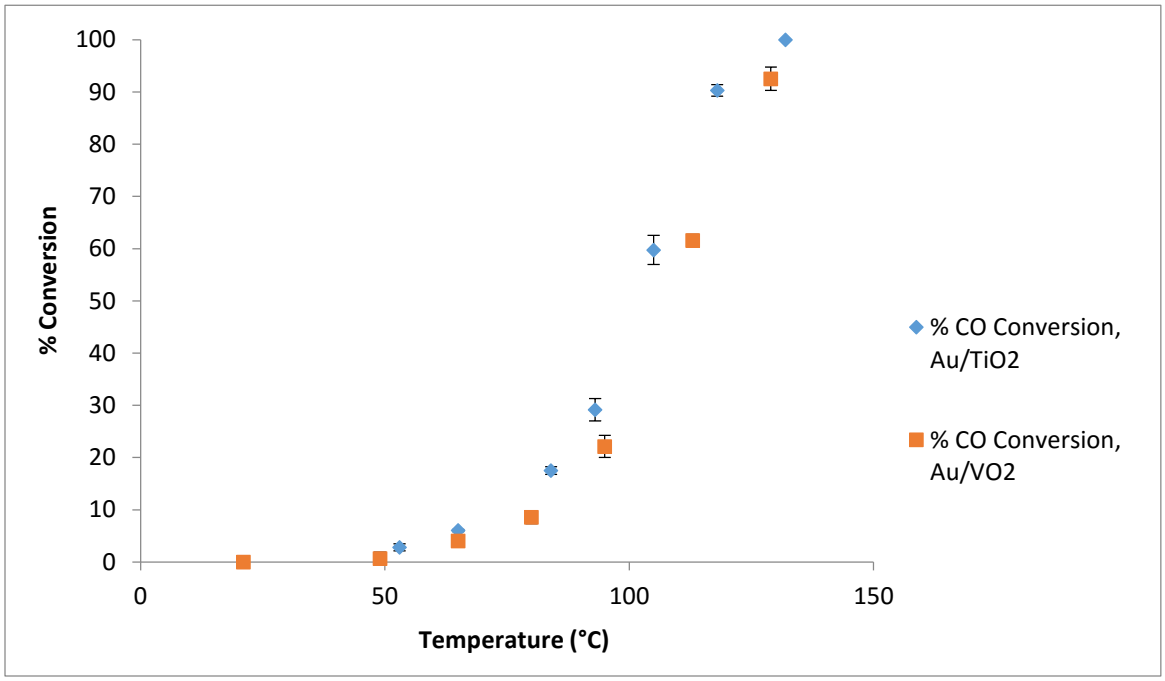

Figure 15. Catalytic activity of Au/TiO_2 and Au/V_2O_4 catalysts prepared using impregnation of MPCs.

Catalytic activity of Au/TiO_2 and Au/V_2O_4 catalysts prepared using MPCs

Due to the deposition-precipitation synthesis producing larger gold particles on the surface of the metal oxide supports, impregnation of MPCs was used as an alternative synthetic method to better control AuNP deposition. By using gold nanoparticles made in a separate synthesis step, the size of the particles can be tailored prior to deposition on the support. To determine the activity of the Au/TiO_2 and Au/V_2O_4 catalysts prepared with MPCs for CO oxidation, the catalysts were tested using the same system as the previous catalysts. As shown in Figure 16, these two catalysts showed very similar activity, with $T_{50\%}$ (Au/TiO_2) = 101 °C and $T_{50\%}$ (Au/VO_2) = 108 °C. This similar value can be attributed to the similarity in gold particle sizes. These values are also close to that of the Au/V_2O_4 catalyst prepared via deposition-precipitation. This was a surprising result, however, because it was expected that these catalysts with gold nanoparticles < 5 nm would show higher activity for CO oxidation.[58,66,68] This discrepancy may be the result of a poorer interfacial connection between the gold nanoparticles and support, due to the nature of the initial MPC adsorption. If so, increasing calcination temperature may serve to better sinter the gold nanoparticles to the support.

Preliminary CO oxidation experiments have been performed using AuNPs deposited on "nano-asterisks" of VO_2. Sample TEM and SEM images of the AuNPs deposited on VO_2 NPs are shown in Figure 15. As can be seen in Figure 17, these initial samples show some of the most promising activity for CO oxidation using vanadium dioxide-supported catalysts - including one batch that demonstrated minimal activity even at room temperature.

Conclusions.

Au/V_2O_4 catalysts were synthesized using either a deposition-precipitation method or through impregnation of monolayer-protected gold nanoparticles. These catalysts showed the ability to oxidize CO with values of $T_{50\%}$ being found at 108°C and 106°C, respectively. These results were compared to Au/TiO_2 catalysts synthesized using identical methods; for deposition-precipitation, the Au/V_2O_4 catalyst was found to require somewhat higher temperatures for comparable catalytic activity. The Au/V_2O_4 and Au/TiO_2 catalysts prepared using impregnation of MPCs showed very similar activity, albeit at temperatures comparable to that of the deposition-precipitation prepared Au/V_2O_4 catalyst.

AuNPs impregnated on VO_2 are currently the most promising catalyst material of the presented results for CO oxidation. However, these catalysts require significant characterization to gain further insight into the interactions of the Au and VO_2 and how this effects the catalytic activity. There have been some reports in the literature that nanostructured gold can be active for CO oxidation without the need of a support.[116–119] It is possible that the impregnation method used in this work did not adequately sinter the AuNPs to the metal oxide supports, and that the gold is the sole source of the catalytic activity seen for those samples, particularly in the case of the impregnation on TiO_2 and V_2O_4.

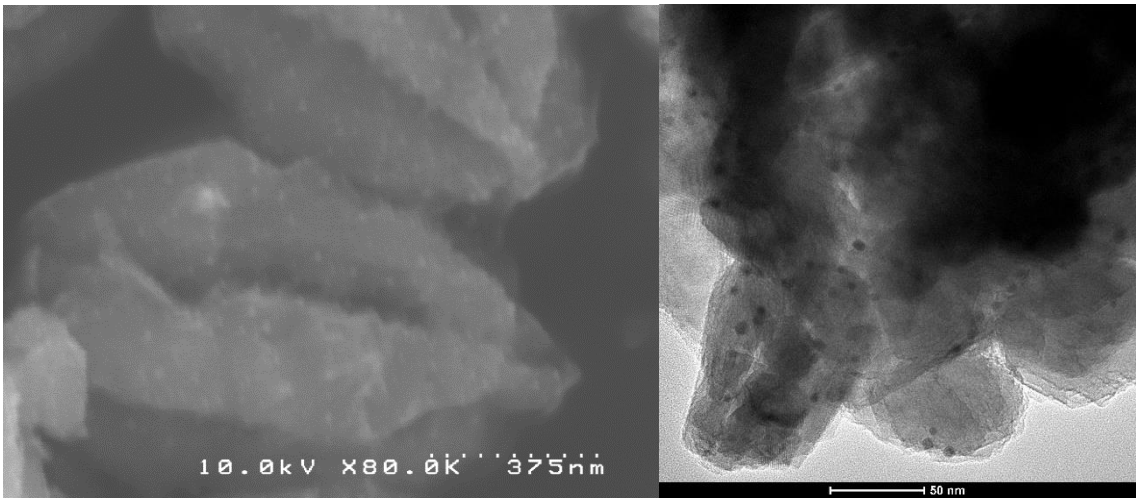

Figure 16. SEM (left) and TEM (right) images of AuNPs deposited on VO_2 NPs.

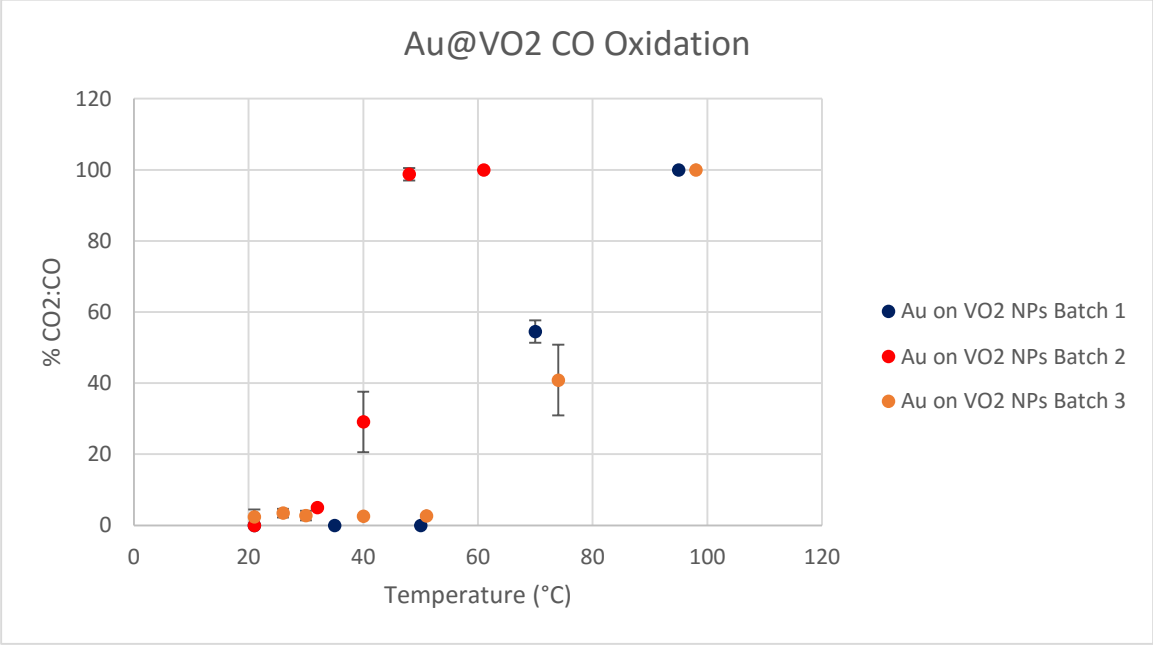

Figure 17. Catalytic activity of initial batches of AuNPs impregnated on VO_2 NPs.

Acknowledgements.

I would like to thank first and foremost Dr. Kenneth Debelak of the Department of Chemical & Biomolecular Engineering at Vanderbilt University, who graciously allowed use of his lab space and instrumentation for the chromatographic measurements. He also was always willing to help me troubleshoot problems (and I had several working with unfamiliar equipment) and give advice. This work was supported by the Defense Threat Reduction Agency, HDTRA 1-10-1-0047.

CHAPTER IV

EXAMINING AU/TIO_2 AND AU/V_2O_4 CATALYSTS FOR THE AEROBIC OXIDATION OF ALCOHOLS

Background.

In Chapter III, the use of vanadium oxide-supported gold catalysts for CO oxidation was discussed. The purpose of the aforementioned study was to determine if vanadium oxide-based catalysts could demonstrate oxidation of CO comparable to other metal oxide-based heterogeneous gold catalysts which had been more thoroughly studied in the context of that reaction. However, heterogeneous gold catalysts have also been well studied for several other reactions, some of which are outlined in Table 2. Of these, selective oxidation of alcohols is a particularly attractive secondary target of study. It remains an important tool in several industrial processes, and the use of heterogeneous gold and transition metal-based catalysts have led to improvements in selectivity, materials, and reaction conditions.[88,120–122]

The primary basis for the following work is a previous report by Karimi and coworkers[122] which used a simple heterogeneous gold catalyst, Au/Cs_2CO_3, in the aerobic oxidation of a variety of benzylic alcohols. They were able to demonstrate high selectivity to the corresponding aldehyde at very mild reaction conditions for several primary benzyl alcohols, offering attractive targets for studying the effectiveness of Au/V_2O_4 catalysts in

systems other than CO oxidation. For this work, 4-methoxybenzyl alcohol was selected as the target of study, due to having the highest reported selectivity as well as being readily available. Furthermore, the expected product, 4-anisaldehyde, is an industrially relevant molecule used for its strong fragrance.[123] Figure 18 shows the proposed oxidation of 4-methoxybenzyl alcohol to this expected product.

Materials and Methods.

Au/V_2O_4 catalysts prepared by deposition-precipitation (as described in Chapter III) were studied in the context of a simple oxidation reaction at very mild conditions.[124] ~50 mg Au/V_2O_4 was slurried in 8 mL toluene in a round bottom flask equipped with a condenser. $O_{2(g)}$ was bubbled through the reaction mixture. 125 µL 4-methoxybenzyl alcohol was added to the mixture and stirred for 24 h. Toluene was removed from the resulting product via rotary evaporation, and the remaining product was redissolved in deuterated chloroform and analyzed via ^1H NMR.

Table 2. Heterogeneous gold catalysts and their uses.

Reaction	Catalyst
Epoxidation of propene[63]	Au on Mesoporous TiO-SiO
Water-gas shift[60]	Au on CeO_2
Selective oxidation of primary alcohols[120]	Au-Pd on TiO_2
Electrooxidation of methanol and CO[125]	Pt-coated Au nanoparticles
Photocatalytic degradation of 4-Chlorophenol[126]	Au on TiO_2
Oxidation of ethanol[121]	Au on various metal oxides[a]
Photocatalytic aerobic oxidation of alcohols[88]	Au on TiO_2
Selective aerobic oxidation of alcohols[122]	Au on Cs_2CO_3

[a]Highest activity supports reported were MnO_2, CeO_2, CuO, Co_3O_4, NiO, ZrO_2, and Fe_2O_3.

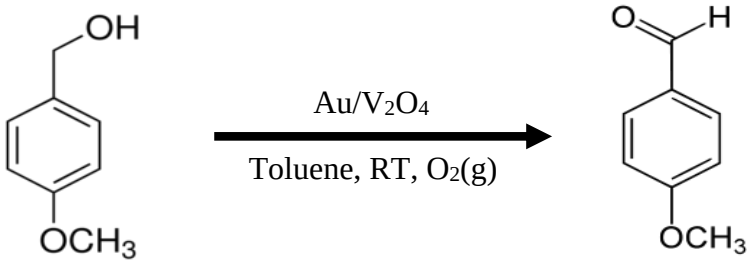

Figure 18. Oxidation of 4-methoxybenzyl alcohol to 4-anisaldehyde (or 4-methoxybenzaldehyde)

Results and Discussion.

In the work of Karimi and coworkers, $NaAuCl_4$ coadded with Cs_2CO_3 was used as the catalyst for the aerobic oxidation of alcohols;[122] this was thus chosen as the positive control for these experiments. They reported that this catalyst gave > 99% yield in the oxidation of 4-methoxybenzyl alcohol to the corresponding aldehyde in O_2. Repeating their method with a similarly made Au/Cs_2CO_3 catalyst, 99% conversion (Figure 19) was seen, which is in agreement with the previously reported results. However, repeating these conditions with an Au/V_2O_4 catalyst showed only 5% conversion to the aldehyde via ^1H NMR (Figure 19). Interestingly, the peak corresponding to the alcohol proton, initially found at $\delta = 3.238$ ppm, has disappeared. Additionally, the peak assigned to the methylene at $\delta = 4.453$ and 4.467 ppm, which is normally split into a doublet by the alcohol proton, has become a singlet, confirming the removal of the alcohol hydrogen. This peak has shifted only slightly downfield to $\delta = 4.529$ ppm, further suggesting that the electron density of the nearby oxygen has slightly increased, corresponding to a slight increase in the deshielding effect on the methylene.

Although it is unclear what this product is, a possible explanation is further oxidation of the aldehyde to a carboxylic acid, which has been seen previously with other heterogeneous gold catalysts.[122,127] However, the data presented here is insufficient to confirm this, as the expected carboxylic acid peak would be too far downfield, and likely would require a higher resolution scan to resolve. If this is the case, then it is possible that shorter reaction times using the Au/V_2O_4 catalyst would lead to a higher yield of the expected aldehyde product. Alternatively, gas chromatography could be used to identify products and yields when using the appropriate internal standards.

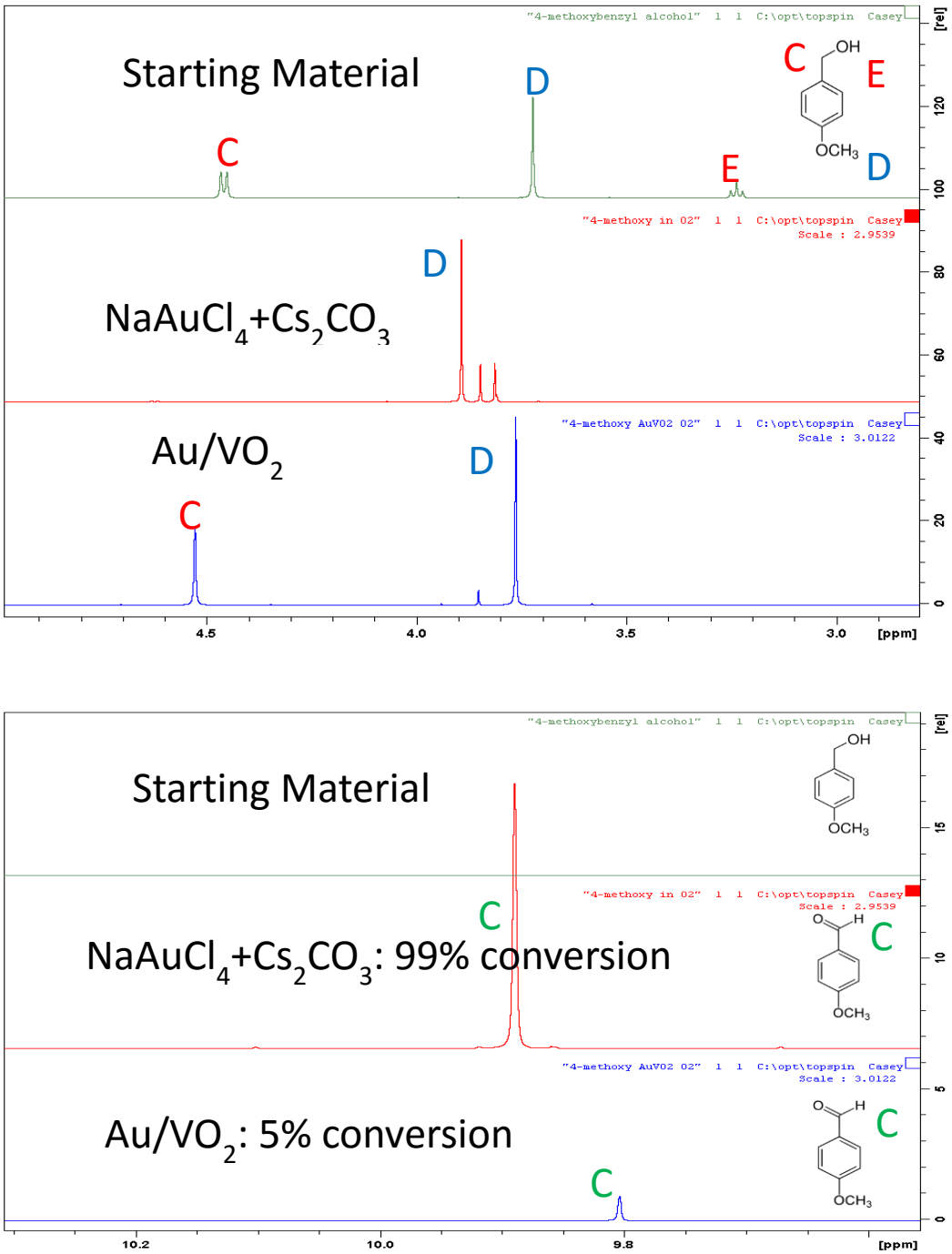

Figure 19. Oxidation of 4-methoxybenzyl alcohol. *Top*: peak corresponding to aldehyde proton can be used as quantitative measure of oxidation by comparing to the peak associated with the 3 hydrogens of the methyl group. *Bottom*: Cs_2CO_3 catalyst shows complete disappearance of the $–CH_2$ and alcohol proton peaks; however, the Au/VO_2 catalyst shows disappearance of only the alcohol proton, with corresponding change of the $–CH_2$ peak to a singlet.

Conclusions.

Au/V_2O_4 catalysts demonstrated minimal oxidation of benzyl alcohols in an aerobic environment, converting only about 5% of the starting material to the expected aldehyde after 24 h. Analysis via ^1H NMR shows another product which was not fully identified, but may be a carboxylic acid formed from further oxidation of the expected aldehyde. By more carefully studying reaction times and anticipating other products, it should be possible to more clearly understand the role of the Au/V_2O_4 catalyst and the associated products in the oxidation of benzyl alcohols.

CHAPTER V

GOLD DEPOSITION ON VANADIUM DIOXIDE FILMS FOR THE ELECTROCHEMICAL REDUCTION OF TNT

Background.

In Chapter II, VO_2 films were shown to electrochemically reduce TNT. However, there have also been reports of gold electrodes[36] and gold nanoparticles[40] being effective in this context. Furthermore, as discussed in Chapter III, gold nanoparticles deposited on vanadium oxide materials have an enhanced effect on the oxidation of carbon monoxide. Therefore, the aim of this research was to determine the effect of depositing gold nanoparticles on films of VO_2 for the electrochemical reduction of TNT.

Experimental.

Synthesis of AuNPs

Hexanethiol-capped gold nanoparticles (AuNPs) were synthesized using the two-phase Brust method.[115] Briefly, 3 eq. tetraoctylammonium bromide (TOAB) was dissolved in toluene and added to aqueous gold acid ($HAuCl_4 \cdot 3H_2O$) in H_2O. The reaction was stirred for 1 h to allow transfer of the gold acid to the toluene. Water was then removed using a separatory funnel. The toluene-soluble reaction was transferred to a chilled flask, and 4 eq.

hexanethiol was added. After 1 min, 10 eq. chilled $NaBH_4$ was quickly added to the reaction to reduce the gold and form the MPCs. After 1.5 h, the toluene was removed via rotary evaporation, followed by addition of ethanol to remove unreacted material overnight. MPCs were then washed with acetonitrile and centrifuged. Washing was repeated 5-10 times prior to drying via rotary evaporation. Tiopronin-capped AuNPs were synthesized using a modified Brust method.[128] Tiopronin and aqueous gold acid were mixed in a 6:1 mixture of methanol:acetic acid in a 3:1 molar ratio for approximately 30 minutes, until the yellow solution had almost turned clear. Then 10 eq. chilled $NaBH_4$ was quickly added to the reaction. The majority of the solvent was removed via rotary evaporation, and the nanoparticles were redissolved in approximately 200 mL H_2O. The pH was adjusted to near 1 with conc. HCl, and then transferred to 10,000 MWCO dialysis tubing and dialyzed against H_2O for 2-3 days. Purity was determined using ^1H NMR. All AuNPs were characterized using transmission electron microscopy (TEM) to determine average nanoparticle diameter.

AuNP deposition onto Vanadium Dioxide Films

In order to deposit AuNPs onto VO_2 films, hexanethiol AuNPs or tiopronin AuNPs were dissolved in an appropriate solvent at a concentration of 1 mg/mL and dropcast onto the film surface after masking the exposed ITO surface. Samples were then calcined under air flow in a tube furnace at 300 °C for 16h.

AuNP characterization

Hexanethiol-capped AuNPs produced had an average size of 2.1±0.5 nm, as shown in Figure 20. Tiopronin-capped AuNPs had an average diameter of 1.9±0.6 nm.

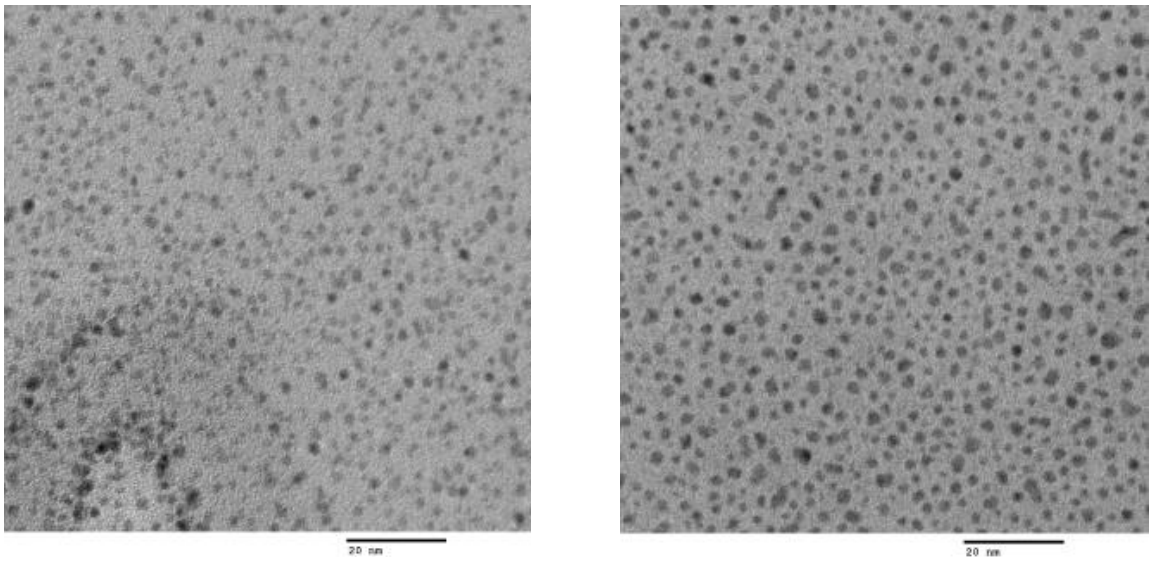

Figure 20. TEM images of **(left)** hexanethiol-capped and **(right)** tiopronin-capped AuNPs. Scale bars are 20 nm.

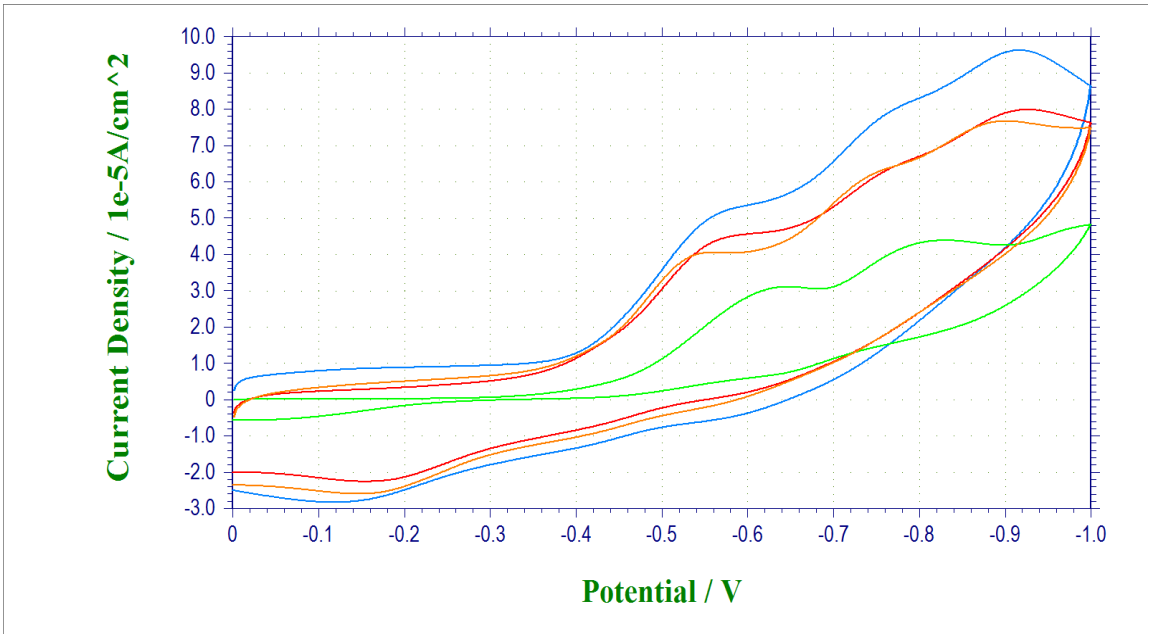

Figure 21. CVs of TNT reduction at 25 ppm for ITO on glass (green), VO_2 on ITO on glass (blue), tiopronin-capped AuNPs on VO_2 film on ITO on glass (orange), and hexanethiol-capped AuNPs on VO_2 film on ITO on glass (red).

Electrochemical Measurements

Cyclic voltammograms were recorded at a potential scan rate of 10 mV s^{-1} in a solution of 0.1 M KCl in H_2O adjusted to pH 8.8 with NaOH. Figure 21 shows a characteristic comparison of ITO on glass, a VO_2 film, TMPCs deposited on a VO_2 film, and C6-MPCs on a VO_2 film, all at 25 ppm TNT. The VO_2 and ITO on glass CVs share the same characteristics that were discussed in Chapter II. The middle curves that correspond to the AuNPs deposited on VO_2 show an interesting similarity that could correlate to the similar size of the AuNPs prior to calcination on the film. Unfortunately, these and similar results show a decreased current response compared to films of VO_2 without AuNPs.

Conclusions.

Deposition of AuNPs on films of VO_2 demonstrated a decrease in current and no enhancement in kinetics compared to the VO_2 films discussed in Chapter II. Therefore, it was determined that the use of AuNPs was not worthwhile in this context.

CHAPTER VI

CONCLUSIONS AND FUTURE DIRECTIONS

The studies discussed in this dissertation demonstrated new uses for vanadium dioxide as a catalytic material by examining its efficacy for known catalysis reactions. In Chapter II, films of vanadium dioxide were successfully used to electrochemically reduce TNT at concentrations as low as 1 μg L^{-1}, which is comparable to the current state-of-the-art limits of detection in the literature. Furthermore, in Chapter V it was shown that the addition of gold nanoparticles to the VO_2 surface does not enhance this activity. The continuation of this work, which is currently underway, is utilizing nanostructured VO_2 such as the "nano-asterisks" described in Chapter III. These should provide new insights into how TNT adsorbs on the surface of the oxide electrode, while also determining the significance of the increased surface area of these particles. Additionally, the nature of the reduction process requires further study to confirm that it is indeed a surface process.

Although these VO_2 nano-asterisks have great promise for catalysis reactions, the study of VO_2 films should not be neglected for these reactions. The phase transition of these particles is not as well characterized, and as long as the goal remains to create a thermocromic or electronic sensor using these materials, thin films deposited on substrates will remain a robust, adaptable method of obtaining such a device.

Gold nanoparticles were deposited on the V_2O_4 precursor powder (normally used as the target for deposition of thin films), as well as VO_2 nano-asterisks, using either

deposition-precipitation (DP) or impregnation of monolayer-protected clusters. In Chapter III, these were used to study the oxidation of carbon monoxide in air. In Chapter IV, they were used in the aerobic oxidation of benzyl alcohols. Although the activity was lower than what has been shown in the literature, both deposition methods produced vanadium oxide-supported gold catalysts that are able to catalyze the oxidation of CO to CO_2. Additionally, the impregnation of MPCs produced more reproducible AuNP sizes on the supports compared to the DP method. By further refining this method, particularly in the calcination step, to optimize AuNP deposition on the nano-asterisks of VO_2, these catalysts may be able to demonstrate a high activity for CO oxidation even at room temperature. Their ability to oxidize benzyl alcohols, however, was less promising and did not merit further study.

These results demonstrate the versatility of vanadium dioxide as an electrode material and catalyst support. Based on this work, further elucidation of the interactions between these materials will lead to the realization of VO_2 as a thermochromic or electronic sensor utilizing the phase transition for a multitude of reactions.

APPENDIX A

SYNTHESIS AND CHARACTERIZATION OF RGD PEPTIDE PRESENTING TIOPRONIN MONOLAYER-PROTECTED CLUSTERS

Background.

Approximately two decades ago, Brust described the synthesis of thiolate capped isolable gold nanoparticles, which offer distinct advantages over traditional colloidal gold particles.[115] These "monolayer-protected clusters" (MPCs) have received significant attention for their stability, simple synthesis, unique size dependent properties, and the ability to functionalize them through place exchange reactions with a wide range of potential ligands,[129] as well as their ability to be repeatedly isolated from and redissolved in a variety of solvents. By using a hydrophilic ligand such as tiopronin (trade name Thiola®, *N*-(2-Mercaptopropionyl)-glycine) (Figure 22), these tiopronin monolayer-protected clusters (TMPCs) become water-soluble, opening large avenues of applicability in biological systems.[128]

Recently, peptides with an arginine-glycine-aspartic acid (RGD) motif have gained some attention due to their ability to mediate targeting and binding to αv integrins of certain tumor endothelium.[130–132] If this RGD motif could be used to functionalize TMPCs, these particles could be used to enhance certain cancer treatment routes including radiation therapy. To this aim, an RGD peptide has been designed with the purpose of

functionalizing a gold nanoparticle to be used to target cancer cells. This peptide was designed to include a cysteine residue separated by a poly(ethylene glycol) (PEG) linker so that it would be able to bind to TMPCs through a place exchange reaction. In order to more closely mimic the secondary structure of RGD-containing peptides, a "looped" form of the RGD-presenting nanoparticles was also designed, in which the RGD motif is exposed in a cyclic manner by attaching the free end of the linear peptide back onto the particle via a coupling reaction to a tiopronin ligand on the particle.

Materials and Methods.

Tetrachloroauric acid trihydrate was synthesized according to established methods[133] and stored at -20°C. *N*-(2-Mercaptopropionyl)-glycine (tiopronin) (Sigma), nitric acid (Fisher Scientific), hydrochloric acid (EMD Chemicals), methanol (Fisher Scientific), glacial acetic acid (Fisher Scientific), deuterium oxide (Cambridge Isotope Laboratories, Inc.), N-(dimethylaminopropyl)-N'-ethylcarbodiimide HCl (EDC) (Sigma), hydroxylamine hydrochloride (Sigma), and N-hydroxysuccinimide (NHS) (Sigma) were all used as received without further purification.

TMPC Synthesis and Characterization

Tiopronin MPCs (TMPCs) were synthesized using a modified Brust synthesis.[115,128] Briefly, 1 g (2.58 mmol) of $HAuCl_4 \bullet 3H_2O$ was codissolved with 7.62 mmol tiopronin (*N*-(2-mercaptopropionyl)glycine) in a 6:1 mixture of methanol:acetic acid. The solution was stirred in an ice bath, and an excess of $NaBH_4$ (51.0 mmol) dissolved in 20 mL water was quickly added to reduce the gold and form the nanoparticles. After stirring

overnight, the solvent was removed by rotary evaporation, and the dry nanoparticles were redissolved in water. Concentrated HCl was added dropwise to the TMPC solution until the pH reached 2.0. This solution was then vacuum filtered through a medium pore sized glass fritted funnel. The filtered solution was transferred to 10,000 MWCO dialysis tubing and placed in a beaker of water and stirred for 1 week, changing the water twice every day. Particles were later dried via rotary evaporation.

An NMR sample was prepared by adding a few drops of deuterium oxide (D_2O) to 500 µL of the dialyzed TMPCs dissolved in deionized water. A Bruker NMR Spectrometer operating at 400 MHz was used to collect the spectrum. A Cary 100 Bio UV-Visible Spectrophotometer was used to obtain an absorbance spectrum of a dilute solution of TMPCs dissolved in deionized water collected over wavelengths 300-700 nm. Pure deionized water was used as a blank. The cuvettes used were 1.5 mL Plastibrand® disposable cuvettes. Thermogravimetric analysis (TGA) was performed on an Instrument Specialist TGA-1000 by heating 2.7558 mg of dry TMPCs to 500°C at a rate of 25°C/min, with a nitrogen flow rate of 60 mL min^{-1}. A Philips CM20 Transmission Electron Microscope (TEM) operating at 200 keV was used to image the particles to determine the size of their gold cores. A dilute solution of TMPCs dissolved in 1 mM HCl was cast onto a mesh copper grid coated with an ultrathin holey carbon film purchased from Ted Pella, Inc. and allowed to dry overnight. Images were taken at 250,000x magnification. The diameters of the particles in each image were determined using ImageJ software (NIH, http://rsb.info.nih.gov/ij/) and an average particle diameter was calculated.

Peptide Synthesis

The RGD peptide was synthesized using a standard Fmoc solid phase peptide synthesis procedure.[134] Most coupling cycles were carried out in a six-fold excess of an aminated C-terminus resin, using Fmoc amino acid/HBTU/HOBt/DIEA (1:1:1:2) in DMF for a minimum of 1 hr. Coupling was carried out in three-fold excess of the resin for 2 hrs. In all cases, Fmoc groups were removed by treatment with 20% piperidine in DMF. Cleaving of the peptide from the resin was achieved by mixing the peptide with a 90% TFA/5% thioanisole/3% anisole/2% EDT solution for 2 hrs. The solution was then filtered through glass wool and precipitated with ether. The peptide was then centrifuged and washed multiple times with ether. The peptide was then purified via HPLC, with collected fractions being analyzed by matrix-assisted laser desorption/ionization mass spectrometry (MALDI-MS).

Place Exchange of RGD Peptide onto TMPCs

Two separate reactions were performed to place exchange (PE) the peptide onto the TMPCs. In the first reaction, 1.72 mg of RGD peptide (1.69 μmol) was dissolved in water and mixed with 40.7 mg (84.6 μmol) TMPCs dissolved in water, resulting in a 50:1 feed ratio of tiopronin:peptide. In the case of "looped" samples, an EDC coupling reaction was used to couple the free carboxylic acid of a tiopronin ligand to the free amine of the RGD peptide. 10 mg of the linear RGD TMPCs were codissolved in 0.1M MES buffer (0.5M NaCl, pH 6.0) with 6 mg EDC and 4 mg NHS (final volume 10 mL) and stirred for 2 hours to allow the activated carboxylic acids to attach to the free peptide amines. Hydroxylamine

hydrochloride (7 mg) was added to quench the reaction, and the looped particles were transferred to 3,500 MWCO dialysis tubing and dialyzed for several days.

Results and Discussion.

TMPC Synthesis and Characterization

An absence of free tiopronin in the TMPC samples was confirmed by 400 MHz NMR. Broadening of tiopronin peaks compared to free tiopronin ligand arises from spin-spin relaxation (T_2) of the ligand attached to the gold core, and is characteristic of TMPC formation.[128] Thermogravimetric analysis provided a percentage of sample weight that can be attributed to the organic tiopronin ligand. It was found that 25.6% by weight of the synthesized particles were tiopronin (Figure 23). A sample TEM image is shown in Figure 24. The results of the imaging reveal an average particle diameter of 1.9±0.7 nm (Figure 25). The UV-Vis spectrum of the TMPCs did not show an absorbance peak at 520 nm, demonstrating a lack of the surface plasmon resonance band that would only be expected for gold nanoparticles approximately 5 nm in diameter and larger.

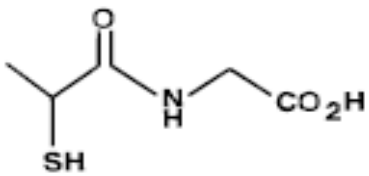

Figure 22. Tiopronin (*N*-(2-Mercaptopropionyl)-glycine)

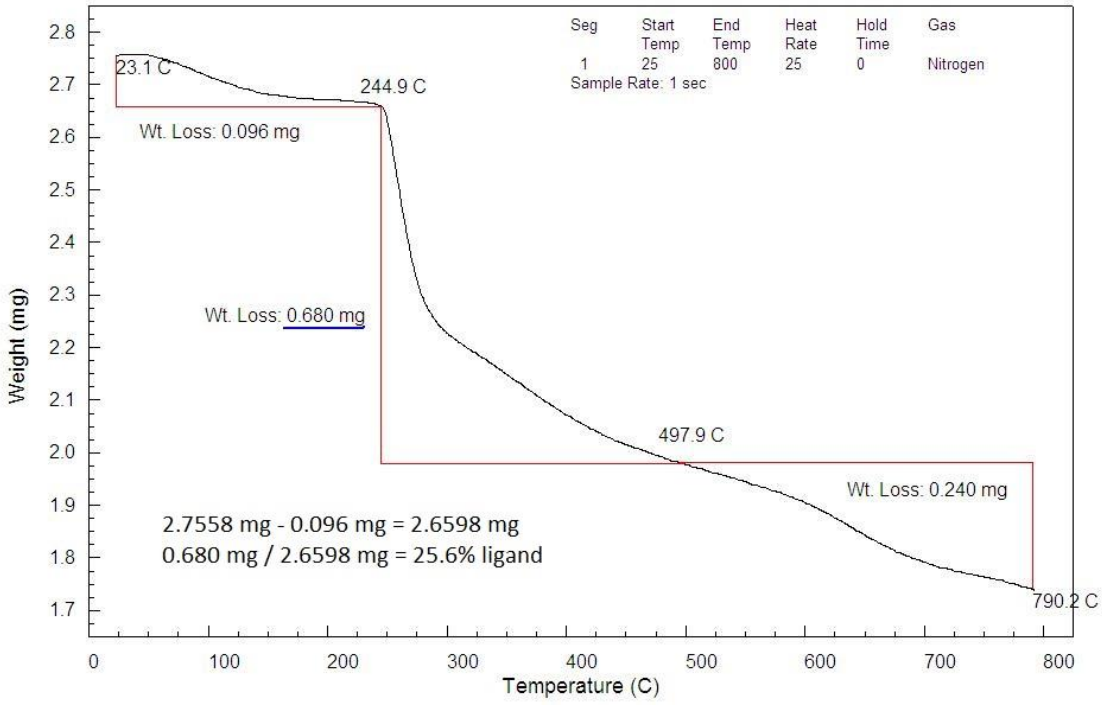

Figure 23. Thermogravimetric analysis of TMPCs. The initial weight loss step is attributed to water. The next weight loss step is attributed to the organic ligand, tiopronin. The final weight loss step is likely due to partial decomposition of the gold core.

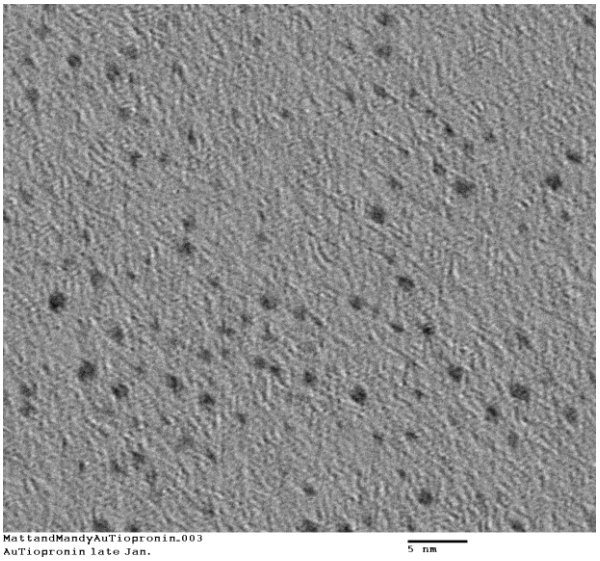

Figure 24. Sample TEM image of TMPCs, average diameter 1.9±0.7 nm. Scale bar represents 5 nm.

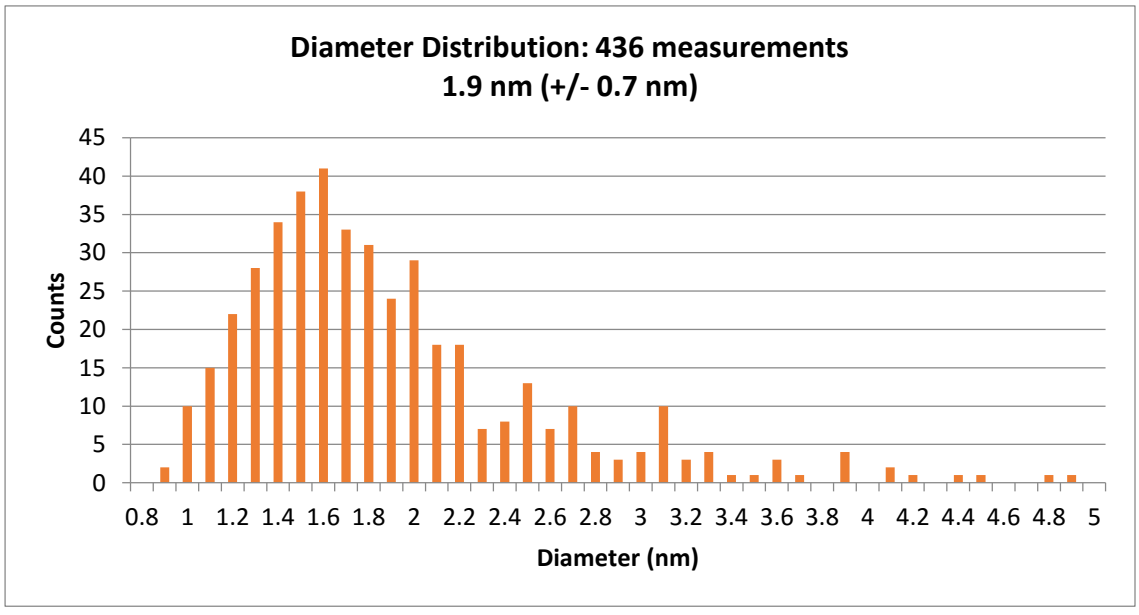

Figure 25. Histogram showing distribution of data for 436 particles measured over 7 TEM images.

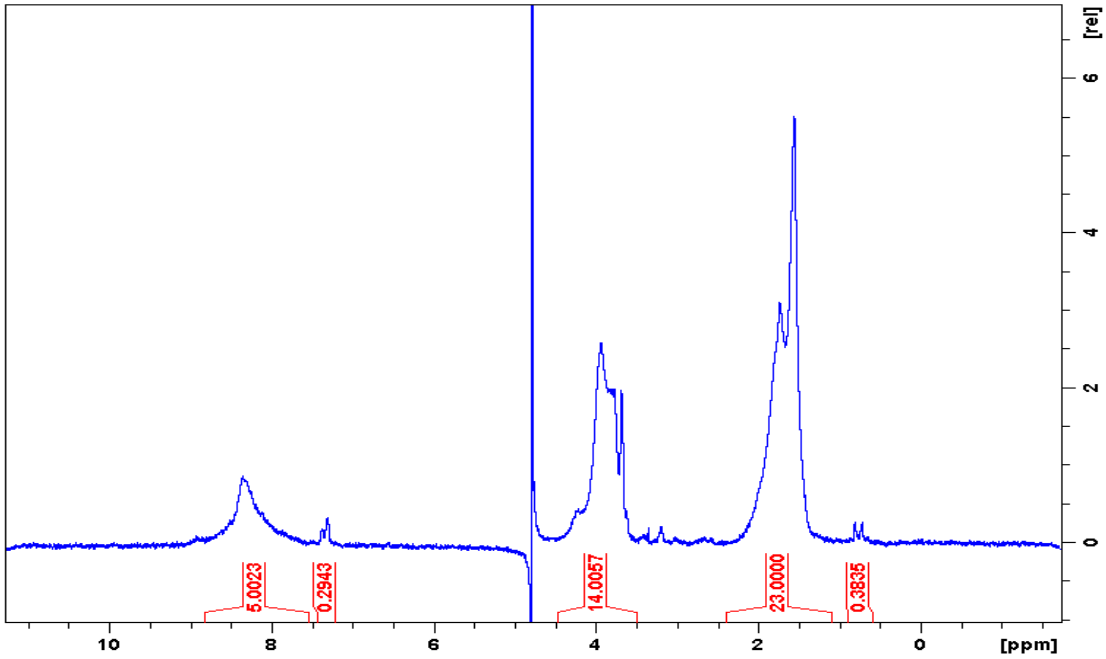

Figure 26. ^{1}H NMR spectrum of RGD-presenting TMPCs. The peaks around 1.5-2 ppm and 3.5-4.5 ppm correspond to the methyl and methylene peaks, respectively. The peak around 8.2 ppm corresponds to the 5 aromatic hydrogens of the phenylalanine residue on the peptide. Integrating this peak to 5 gives a methyl peak integration of 23; this gives a tiopronin:peptide ratio of 7.6:1.

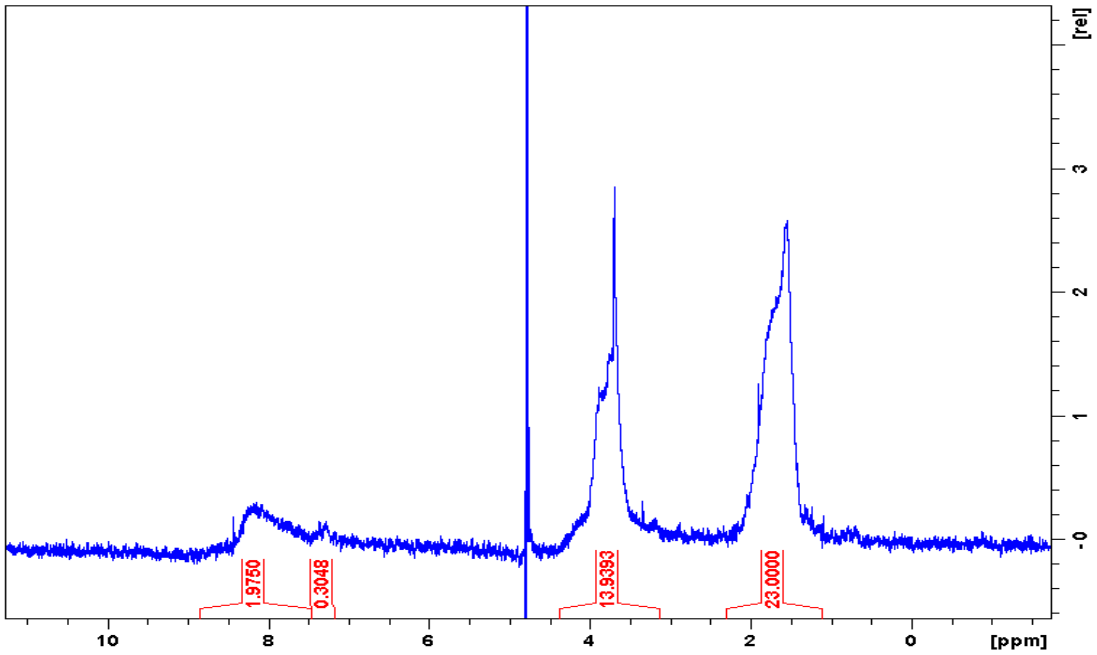

Figure 27. ^{1}H NMR of "looped" RGD-presenting TMPCs. The methyl : phenylalanine peak ratio has decreased from 23:5 in the linear RGD TMPCs to 23:2, giving a new tiopronin:peptide ratio of 19:1, and thus only 4 peptides per particle.

Matrix-Assisted Laser Desorption/Ionization-Mass Spectrometry **(**MALDI-MS) was used to confirm the successful synthesis of the RGD peptide. Two major masses were identified at $[M+H]^+$ 1030 Da and $[2M-H]^+$ 2058 Da, the latter corresponding to an oxidized dimer (disulfide bridge of two cysteines). Confirmation of peptide binding to TMPCs was confirmed by ^{1}H NMR (Figure 26). An approximate tiopronin:peptide ratio of 7.6:1 was found, giving an average of 10-11 peptides per particle.

^{1}H NMR was further used to attempt to confirm looping of the RGD peptides (Figure 27). A new ratio of ca. 4 peptides per particle was found for this sample, but it was unclear whether this points to actual looping of the peptide onto the particles or some other phenomenon.

Conclusions.

In this study, RGD-presenting TMPCs were synthesized and secondary structure in the form of "looped" peptide was attempted. However, the extent of "looping" of the RGD peptide was unclear. As a result of this study, efforts in the Cliffel laboratory have begun to examine both linear and looped RGD-TMPCs and their effect on the radiosensitivity of cells.

APPENDIX B

ANALYSIS OF BINDING AND PHOTOOXIDATION OF THIOLS ON GOLD USING QCM AND FTIR

Background.

As mentioned previously, one of the long-term goals of this work was to determine the viability of VO_2-based materials as sensing platforms for reactions such as the catalytic decomposition of TNT. Such a sensor would utilize the enthalpy of reaction to induce a thermochromic response as the mode of detection, and thus would be particularly useful in detecting high-energy molecules such as TNT that release a significant amount of heat upon decomposition. In this same vein, the decomposition of these molecules results in no residual adsorbants on the surface, making the surface "self-decontaminating". However, for those reactions in which complete decomposition does not occur, some other method of removing the reactants must be employed. One way to accomplish this is through UV irradiation of the surface. This could be particularly useful in the photooxidation of thiol molecules on gold, which is particularly important due to the high affinity of thiol compounds for gold.[135–137] In this study, a quartz crystal microbalance (QCM) was used to measure the desorption of self-assembled monolayers (SAMs) on a gold electrode on quartz crystal.

The QCM consists of a quartz piezoelectric resonator with a metal electrode wrapped around it. This combination of electrode and resonator is attached to an oscillator circuit. It has become a useful analytical technique due to the linear relationship between deposited mass and the frequency of the crystal resonance.[138] The ideal oscillator for this is quartz because it has desirable mechanical, electrical, chemical, and thermal properties.[139] Specifically, AT-cut quartz crystals have a temperature coefficient that is nearly zero between 0 and 50 ºC, making them ideal for QCM measurements at ambient temperatures without the need for temperature control.[36]

In order to make mass loading calculations using the QCM, the following relationship (proposed by Sauerbrey[138] and henceforth named the Sauerbrey equation) between mass and frequency shift becomes useful (equation 1):

$$\Delta f = C_f \Delta m$$

where Δf is the frequency shift of the quartz crystal in Hz, Δm is the mass loaded onto the crystal in kg, and C_f is known as Sauerbrey's sensitivity factor and is in units of Hz kg^{-1}.[138] Sauerbrey's sensitivity factor is defined by the following equation (equation 2):

$$C_f = \frac{-2 f_0^{\,2}}{A\sqrt{\rho_q \mu_q}}$$

where f_0 is the first harmonic resonant frequency of the unloaded crystal in Hz, A is the active area of the QCM crystal in m^2, ρ_q is the density of quartz (2.648 kg/m^3) and μ_q is the shear modulus of AT-cut quartz (2.95 x 10^{11} N/cm^2).[34,37] The sensitive area is the overlap area of the large front electrode with the small rear electrode, 0.3419 cm^2. The C_f for a 5 MHz crystal is 0.0566 Hz $cm^2/\mu g$.

Materials and Methods.

QCM experiments were performed with a Maxtek RQCM Quartz Crystal Microbalance with all channels tuned to 5 MHz, and 1 inch 5 MHz Quartz Crystals with gold-plated chromium electrodes were purchased from Maxtek. 1-Hexanethiol (Acros Organics) was used as received. UV irradiation was performed (254 nm) using a Mineralight® UV Lamp (UVP) in short wave mode.

In a typical experiment, crystals were first cleaned with Piranha (3 H_2SO_4 : 1 H_2O_2), then rinsed with deionized water, ethanol, and dried with cool nitrogen. This was repeated two more times, and in some cases followed by 10 minutes of cleaning by ozone. Clean crystals were then secured in their holders and connected to the channels on the RQCM. Once the holders were placed in the chamber and the chamber was sealed, the channels were locked and the data recording software was started. After an initial period (>15 min) to allow instrument drift to minimize, recording was started. After some time, 1-hexanethiol was added to a 3-neck flask connected upstream and allowed to evaporate. These vapors were carried into the chamber using ambient air pumped by a gear pump as a carrier gas. After allowing the thiols to bind to the gold (typically 1 hour), the crystals were exposed to UV radiation from a UV lamp for 1 hr.

Results and Discussion.

In the initial experiment performed, 200 µL 1-hexanethiol was injected ca. 20 minutes after reaching a steady baseline signal. The large UV lamp was turned on 1 hour later. After another hour, the lamp was turned back off. The results (Figure 28) suggested that the large UV lamp was having an adverse effect on the experiment. Thus, a control experiment was conducted using the large UV lamp as well as a smaller handheld UV lamp. Figure 29 shows that the large UV lamp does cause a significant amount of drift in the instrument, most likely due to a temperature change in the crystal (an atmospheric temperature increase of 8°C was measured directly above the quartz crystals). A smaller power UV lamp was therefore used for another control. This lamp in short wave mode (254 nm) caused a much smaller amount of drift compared to the large lamp. A comparison of the two controls is shown in Figure 30. The small UV lamp, which shows much less drift, was thus used for the remainder of the experiments.

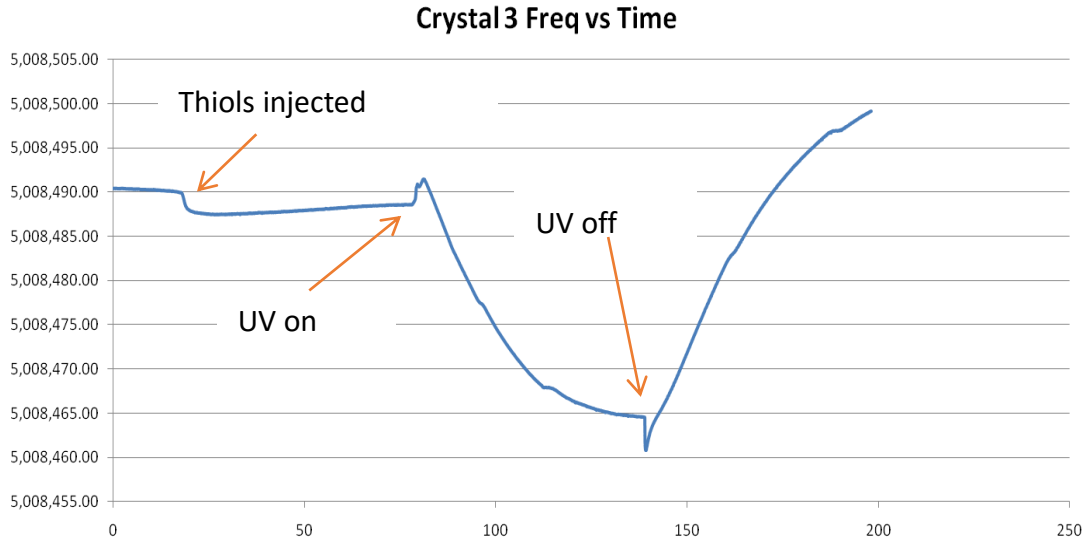

Figure 28. Measurement of the frequency of the quartz crystal over time. When the large UV Lamp is turned on, a large decrease in frequency is observed (after an intial spike due to electrical noise).

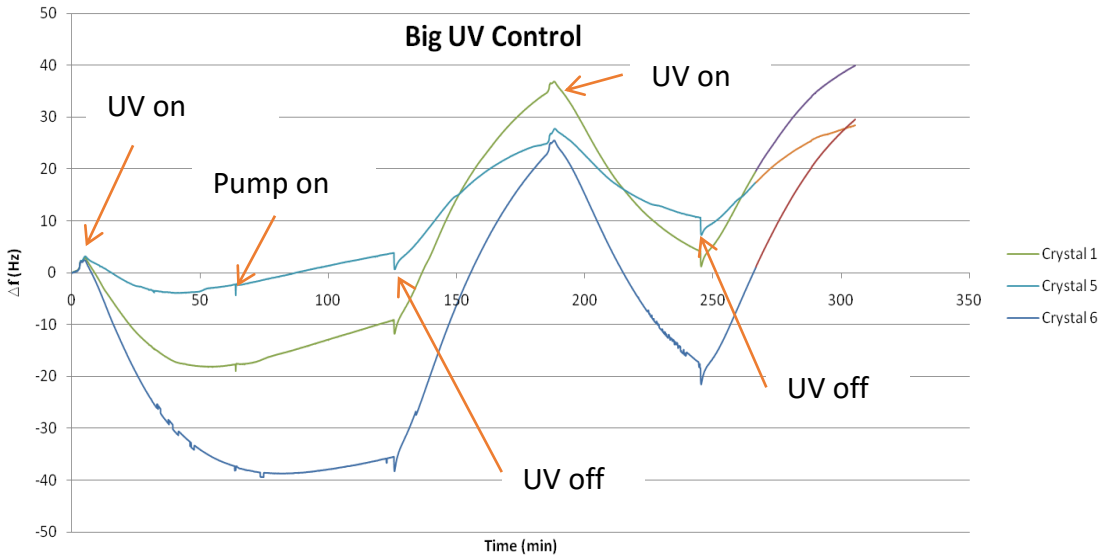

Figure 29. Control experiment for the large UV lamp. The large frequency changes suggest that this lamp is not suited for this application.

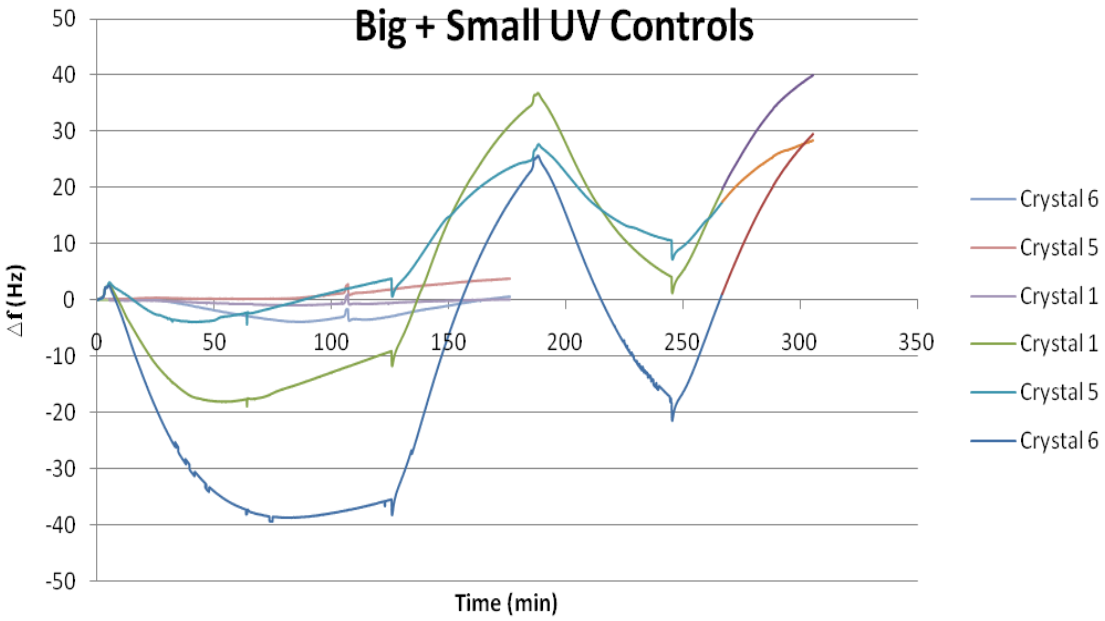

Figure 30. Comparison of the large and small UV lamps. The frequency changes of the small lamp are much smaller than those of the large UV lamp.

The effectiveness of the small UV lamp on the photooxidation of thiols on the QCM crystals was then tested. Using a similar procedure to that described above for the large UV lamp, thiols were given 1.5 hrs to bind to the crystal before the UV lamp was turned on. However, outside of instrument drift there seemed to be no frequency change corresponding to a mass increase on the crystal.

A series of control studies were performed to determine the cause of the drift. It was found that initial drift could be minimized by allowing the instrument to run for 8 hours, at which point the frequency remained almost constant. It was noticed, however, that the light from the fume hood caused a downward drift in the frequency when turned on (and a subsequent upward drift when turned back off). This was thought to be due to the instrument being on the same electrical circuit as the light. Therefore, the change in frequency was monitored with a set of battery operated light sources. It was discovered that even incandescent light from a flashlight causes distinct changes in the frequency of the crystal, and the crystals are immediately responsive to exposure and covering (data not shown).

Conclusions.

Initial experiments to determine the effect of UV irradiation on SAMs were inconclusive due to multiple sources of noise that arose from the high sensitivity of the QCM. If this study were to be revisited, it may be more beneficial to utilize different surface techniques, such as polarization-modulation FTIR, to analyze molecules on the surface.

REFERENCES

(1) Morin, F. J. *Phys. Rev. Lett.* **1959**, *3* (1), 34–36.

(2) Manning, T.; Parkin, I.; Pemble, M.; Sheel, D.; Vernardou, D. *Chem. Mater.* **2004**, *16* (13), 744–749.

(3) Nag, J.; Haglund Jr, R. F. *J. Phys. Condens. Matter* **2008**, *20* (26), 264016.

(4) Warnick, K. H.; Wang, B.; Cliffel, D. E.; Wright, D. W.; Haglund, R. F.; Pantelides, S. T. *Nano Lett.* **2013**, *13* (2), 798–802.

(5) Wu, C.; Feng, F.; Xie, Y. *Chem. Soc. Rev.* **2013**, *42* (12), 5157–5183.

(6) Takei, H.; Koide, S. *J. Phys. Soc. Japan* **1968**, *24* (6), 1394.

(7) Fuls, E. N.; Hensler, D. H.; Ross, a. R. *Appl. Phys. Lett.* **1967**, *10* (7), 199–201.

(8) Borek, M.; Qian, F.; Nagabushnam, V.; Singh, R. K. *Appl. Phys. Lett.* **1993**, *63* (24), 3288–3290.

(9) Chae, B.-G.; Kim, H.-T.; Yun, S.-J.; Kim, B.-J.; Lee, Y.-W.; Youn, D.-H.; Kang, K.-Y. *Electrochem. Solid-State Lett.* **2006**, *9* (1), C12–C14.

(10) Marvel, R. E.; Appavoo, K.; Choi, B. K.; Nag, J.; Haglund, R. F. *Appl. Phys. A* **2012**, *111* (3), 975–981.

(11) Suh, J. Y.; Lopez, R.; Feldman, L. C.; Haglund, R. F. *J. Appl. Phys.* **2004**, *96* (2), 1209–1213.

(12) Wu, C.; Zhang, X.; Dai, J.; Yang, J.; Wu, Z.; Wei, S.; Xie, Y. *J. Mater. Chem.* **2011**, *21* (12), 4509–4517.

(13) Son, J.-H.; Wei, J.; Cobden, D.; Cao, G.; Xia, Y. *Chem. Mater.* **2010**, *22* (10), 3043–3050.

(14) Ji, S.; Zhang, F.; Jin, P. *Sol. Energy Mater. Sol. Cells* **2011**, *95* (12), 3520–3526.

(15) van der Pauw, L. J. *Philips Technical Review*. 1958, pp 220–224.

(16) van der Pauw, L. J. *Philips Res. Reports* **1958**, *13* (1), 1–11.

(17) Shi, J.; Zhou, S.; You, B.; Wu, L. *Sol. Energy Mater. Sol. Cells* **2007**, *91* (19), 1856–1862.

(18) Jeong, J.; Aetukuri, N.; Graf, T.; Schladt, T. D.; Samant, M. G.; Parkin, S. S. P. *Science (80-.).* **2013**, *339* (6126), 1402–1405.

(19) Wang, J. *Electroanalysis* **2007**, *19* (4), 415–423.

(20) Yinon, J. *TrAC Trends Anal. Chem.* **2002**, *21* (4), 292–301.

(21) Lewis, T. A.; Newcombe, D. A.; Crawford, R. L. *J. Environ. Manage.* **2004**, *70* (4), 291–307.

(22) Pennington, J. C.; Brannon, J. M. *Thermochim. Acta* **2002**, *384* (1–2), 163–172.

(23) Amaral, H. I. F.; Fernandes, J.; Berg, M.; Schwarzenbach, R. P.; Kipfer, R. *Chemosphere* **2009**, *77* (6), 805–812.

(24) Marinovic‡, V.; Marinovic‡, S.; Jovanovic‡, M.; Jovanovic‡, J.; Strbac, S. *J. Electroanal. Chem.* **2010**, *648* (1), 1–7.

(25) de Sanoit, J.; Vanhove, E.; Mailley, P.; Bergonzo, P. *Electrochim. Acta* **2009**, *54* (24), 5688–5693.

(26) Hrapovic, S.; Majid, E.; Liu, Y.; Male, K.; Luong, J. H. T. *Anal. Chem.* **2006**, *78* (15), 5504–5512.

(27) Palaniswamy, D. K.; Sorial, G. A.; Maloney, S. W. *Environ. Eng. Sci.* **2004**, *21* (2), 203–218.

(28) Sabbioni, G.; Sepai, O.; Norppa, H.; Yan, H.; Hirvonen, a; Zheng, Y.; Järventaus,

H.; Bäck, B.; Brooks, L. R.; Warren, S. H.; Demarini, D. M.; Liu, Y. Y. *Biomarkers* **2007**, *12* (1), 21–37.

(29) Ayoub, K.; van Hullebusch, E. D.; Cassir, M.; Bermond, A. *J. Hazard. Mater.* **2010**, *178*, 10–28.

(30) Chua, C. K.; Pumera, M.; Rulisek, L. *J. Phys. Chem. C* **2012**, *116* (6), 4243–4251.

(31) Wang, J.; Bhada, R. K.; Lu, J.; MacDonald, D. *Anal. Chim. Acta* **1998**, *361*, 85–91.

(32) Wang, J.; Hocevar, S. B.; Ogorevc, B. *Electrochem. commun.* **2004**, *6* (2), 176–179.

(33) Toh, H. S.; Ambrosi, A.; Pumera, M. *Catal. Sci. Technol.* **2013**, *3* (1), 123–127.

(34) Goh, M.; Pumera, M. *Anal. Bioanal. Chem.* **2010**, *399* (1), 127–131.

(35) Riskin, M.; Tel-Vered, R.; Bourenko, T.; Granot, E.; Willner, I. *J. Am. Chem. Soc.* **2008**, *130* (30), 9726–9733.

(36) Wen, R.; Zhang, H.-X.; Yan, C.-J.; Yan, H.-J.; Pan, G.-B.; Wan, L.-J. *Chem. Commun. (Cambridge, United Kingdom)* **2008**, *0* (16), 1877–1879.

(37) Bozic, R. G.; West, A. C.; Levicky, R. *Sensors Actuators B Chem.* **2008**, *133* (2), 509–515.

(38) Schmelling, D. C.; Gray, K. A.; Kamat, P. V. *Environ. Sci. Technol.* **1996**, *30* (8), 2547–2555.

(39) Grigoriants, I.; Markovsky, B.; Persky, R.; Perelshtein, I.; Gedanken, A.; Aurbach, D.; Filanovsky, B.; Bourenko, T.; Felner, I. *Electrochim. Acta* **2008**, *54* (2), 690–697.

(40) Filanovsky, B.; Markovsky, B.; Bourenko, T.; Perkas, N.; Persky, R.; Gedanken, A.; Aurbach, D. *Adv. Funct. Mater.* **2007**, *17* (9), 1487–1492.

(41) Trammell, S. A; Zeinali, M.; Melde, B. J.; Charles, P. T.; Velez, F. L.; Dinderman, M. A; Kusterbeck, A.; Markowitz, M. A. *Anal. Chem.* **2008**, *80* (12), 4627–4633.

(42) Trammell, S. A.; Velez, F.; Charles, P. T.; Kusterbeck, A. *Anal. Lett.* **2008**, *41* (14), 2634–2645.

(43) Pittman, T. L.; Thomson, B.; Miao, W. *Anal. Chim. Acta* **2009**, *632* (2), 197–202.

(44) Olivetti, E. A.; Avery, K. C.; Taniguchi, I.; Sadoway, D. R.; Mayes, A. M. *J. Electrochem. Soc.* **2008**, 488–493.

(45) Dong, W.; Sakamoto, J. S.; Dunn, B. *Sci. Technol. Adv. Mater.* **2003**, *4* (1), 3–11.

(46) Tranchant, A.; Messina, R.; Perichon, J. *J. Electroanal. Chem.* **1980**, *113*, 225–232.

(47) Spahr, M. E.; Stoschitzki-bitterli, P.; Nesper, R.; Haas, O.; Novák, P. *J. Electrochem. Soc.* **2000**, *146* (8), 2780–2783.

(48) Ozer, N. *Thin Solid Films* **1997**, *305*, 80–87.

(49) Livage, J. *Chem. Mater.* **1991**, *3* (8), 578–593.

(50) Li, S.-Y.; Niklasson, G. a.; Granqvist, C. G. *J. Appl. Phys.* **2014**, *115* (5), 053513.

(51) Wall, S.; Foglia, L.; Wegkamp, D.; Appavoo, K.; Nag, J.; Haglund, R.; Stähler, J.; Wolf, M. *Phys. Rev. B* **2013**, *87* (11), 115126.

(52) Zhou, X.-T.; Ji, H.-B.; Huang, X.-J. *Molecules* **2012**, *17* (2), 1149–1158.

(53) Pashkin, a.; Kübler, C.; Ehrke, H.; Lopez, R.; Halabica, a.; Haglund, R. F.; Huber, R.; Leitenstorfer, a. *Phys. Rev. B* **2011**, *83* (19), 195120.

(54) Yang, Z.; Ko, C.; Ramanathan, S. *Annu. Rev. Mater. Res.* **2011**, *41* (1), 337–367.

(55) Seo, M.; Kyoung, J.; Park, H.; Koo, S.; Kim, H.; Bernien, H.; Kim, B. J.; Choe, J. H.; Ahn, Y. H.; Kim, H.-T.; Park, N.; Park, Q.-H.; Ahn, K.; Kim, D. *Nano Lett.*

2010, *10* (6), 2064–2068.

(56) Paik, T.; Hong, S.; Gaulding, E. A.; Caglayan, H.; Gordon, T. R.; Engheta, N.; Kagan, C. R.; Murray, C. B. *ACS Nano* **2013**

(57) Kalvoda, R.; Kopanica, M. *Pure Appl. Chem.* **1989**, *61* (1), 97–112.

(58) Bond, G. C. *Catal. Today* **2002**, *72* (1-2), 5–9.

(59) Bond, G. C.; Sermon, P. A.; Webb, G.; Buchanan, D. A.; Wells, P. B. *J. Chem. Soc. Chem. Commun.* **1973**, No. 13, 444b – 445.

(60) Haruta, M.; Kobayashi, T.; Sano, H.; Yamada, N. *Chem. Lett.* **1987**, 405–408.

(61) Torres Sanchez, R. M.; Ueda, A.; Tanaka, K.; Haruta, M. *J. Catal.* **1997**, *168* (1), 125–127.

(62) Fu, Q.; Weber, A.; Flytzani-Stephanopoulos, M. *Catal. Letters* **2001**, *77* (1), 87–95.

(63) Sinha S.; Tsubota, S.; Haruta, M., A. K. . S. *Top. Catal.* **2004**, *29* (3-4), 95–102.

(64) Hashmi, A. S. K.; Hutchings, G. J. *Angew. Chemie Int. Ed.* **2006**, *45* (47), 7896–7936.

(65) Hutchings, G. J.; Haruta, M. *Appl. Catal. A Gen.* **2005**, *291* (1-2), 2–5.

(66) Bond, G. C.; Thompson, D. T. *Gold Bull.* **2000**, *33*, 41–51.

(67) Hutchings, G. J.; Brust, M.; Schmidbaur, H. *Chem. Soc. Rev.* **2008**, *37* (9), 1759–1765.

(68) Haruta, M. *CATTECH* **2002**, *6* (3), 102–115.

(69) Bond, G. C.; Thompson, D. T. *Catal. Rev.* **1999**, *41* (3-4), 319–388.

(70) Tsubota, S.; Haruta, M.; Kobayashi, T.; Ueda, A.; Nakahara, Y.; G. Poncelet, P. A. J. P. G.; Delmon, B. In *Studies in Surface Science and Catalysis*; Elsevier, 1991; Vol. Volume 63, pp 695–704.

(71) Lin, H.-Y.; Chen, Y.-W. *Ind. Eng. Chem. Res.* **2005**, *44* (13), 4569–4576.

(72) Daniells, S. T.; Overweg, A. R.; Makkee, M.; Moulijn, J. A. *J. Catal.* **2005**, *230* (1), 52–65.

(73) Kobayashi, T.; Haruta, M.; Tsubota, S.; Sano, H.; Delmon, B. *Sensors Actuators B Chem.* **1990**, *1*, 222–225.

(74) Okumura, M.; Tanaka, K.; Ueda, A.; Haruta, M. *Solid State Ionics* **1997**, *95*, 143–149.

(75) Lee, S.J.; Gavriilidis, A. *J. Catal.* **2002**, *206* (2), 305–313.

(76) Haruta, M.; Yamada, N.; Kobayashi, T.; Iijima, S. *J. Catal.* **1989**, *115* (2), 301–309.

(77) Li, W.C.; Comotti, M.; Schüth, F. *J. Catal.* **2006**, *237* (1), 190–196.

(78) Zheng, N.; Stucky, G. D. *J. Am. Chem. Soc.* **2006**, *128* (44), 14278–14280.

(79) Long, C. G.; Gilbertson, J. D.; Vijayaraghavan, G.; Stevenson, K. J.; Pursell, C. J.; Chandler, B. D. *J. Am. Chem. Soc.* **2008**, *130* (31), 10103–10115.

(80) Hartshorn, H.; Pursell, C. J.; Chandler, B. D. *J. Phys. Chem. C* **2009**, *113* (24), 10718–10725.

(81) Kahlich, M. J.; Gasteiger, H. A.; Behm, R. J. *J. Catal.* **1999**, *182* (2), 430–440.

(82) Schubert, M. M.; Hackenberg, S.; van Veen, A. C.; Muhler, M.; Plzak, V.; Behm, R. J. *J. Catal.* **2001**, *197* (1), 113–122.

(83) Carrettin, S.; Concepción, P.; Corma, A.; López Nieto, J. M.; Puntes, V. F. *Angew. Chemie Int. Ed.* **2004**, *43* (19), 2538–2540.

(84) Hernández, J. A.; Gómez, S. A.; Zepeda, T. A.; Fierro-González, J. C.; Fuentes, G. a. *ACS Catal.* **2015**, 4003–4012.

(85) Guzman, J.; Corma, A. *Chem. Commun. (Cambridge, United Kingdom)* **2005**, No. 6, 743–745.

(86) Veith, G. M.; Lupini, A. R.; Rashkeev, S.; Pennycook, S. J.; Mullins, D. R.; Schwartz, V.; Bridges, C. A.; Dudney, N. J. *J. Catal.* **2009**, *262* (1), 92–101.

(87) Rombi, E.; Cutrufello, M. G.; Monaci, R.; Cannas, C.; Gazzoli, D.; Onida, B.; Pavani, M.; Ferino, I. *J. Mol. Catal. A Chem.* **2015**, *404-405*, 83–91.

(88) Tsukamoto, D.; Shiraishi, Y.; Sugano, Y.; Ichikawa, S.; Tanaka, S.; Hirai, T. *J. Am. Chem. Soc.* **2012**, *134* (14), 6309–6315.

(89) Green, I. X.; Tang, W.; McEntee, M.; Neurock, M.; Yates, J. T. *J. Am. Chem. Soc.* **2012**.

(90) Ma, Z.; Dai, S. *Nano Res.* **2011**, *4* (1), 3–32.

(91) Laoufi, I.; Saint-Lager, M. C.; Lazzari, R.; Jupille, J.; Robach, O.; Garaude, S.; Cabailh, G.; Dolle, P.; Cruguel, H.; Bailly, A. *J. Phys. Chem. C* **2011**, null – null.

(92) Green, I. X.; Tang, W.; Neurock, M.; Yates, J. T. *Science (80-.).* **2011**, *333* (6043), 736–739.

(93) Lopez-Acevedo, O.; Kacprzak, K. A.; Akola, J.; HÃ¤kkinen, H. *Nat Chem* **2010**, *2* (4), 329–334.

(94) Sangeetha, P.; Chang, L.-H.; Chen, Y.-W. *Mater. Chem. Phys.* **2009**, *118* (1), 181–186.

(95) Dozzi, M. V.; Prati, L.; Canton, P.; Selli, E. *Phys. Chem. Chem. Phys.* **2009**, *11* (33), 7171–7180.

(96) Rashkeev, S. N.; Lupini, A. R.; Overbury, S. H.; Pennycook, S. J.; Pantelides, S.

T. *Phys. Rev. B* **2007**, *76* (3), 35438.

(97) Ma, Z.; Overbury, S. H.; Dai, S. *J. Mol. Catal. A Chem.* **2007**, *273* (1-2), 186–197.

(98) Hayden, B. E.; Pletcher, D.; Suchsland, J.-P. *Angew. Chemie Int. Ed.* **2007**, *46* (19), 3530–3532.

(99) Zhu, H.; Ma, Z.; Overbury, S.; Dai, S. *Catal. Letters* **2007**, *116* (3), 128–135.

(100) Moreau, F.; Bond, G. C. *Appl. Catal. A Gen.* **2006**, *302* (1), 110–117.

(101) Zanella, R.; Delannoy, L.; Louis, C. *Appl. Catal. A Gen.* **2005**, *291* (1-2), 62–72.

(102) Soares, J. M. C.; Bowker, M. *Appl. Catal. A Gen.* **2005**, *291* (1â€“2), 136–144.

(103) Zanella, R.; Giorgio, S.; Shin, C.-H.; Henry, C. R.; Louis, C. *J. Catal.* **2004**, *222* (2), 357–367.

(104) Chen, M. S.; Goodman, D. W. *Science.* **2004**, *306* (5694), 252–255.

(105) Lee, S.; Fan, C.; Wu, T.; Anderson, S. L. *J. Am. Chem. Soc.* **2004**, *126* (18), 5682–5683.

(106) Moreau, F.; Bond, G. C.; Taylor, A. O. *Chem. Commun. (Cambridge, United Kingdom)* **2004**, No. 14, 1642–1643.

(107) Centeno, M.; Carrizosa, I.; Odriozola, J. A. *Appl. Catal. A Gen.* **2003**, *246* (2), 365–372.

(108) Boccuzzi, F.; Chiorino, A.; Manzoli, M.; Lu, P.; Akita, T.; Ichikawa, S.; Haruta, M. *J. Catal.* **2001**, *202* (2), 256–267.

(109) Boccuzzi, F.; Chiorino, A. *J. Phys. Chem. B* **2000**, *104* (23), 5414–5416.

(110) Sobczak, J. W.; Andreeva, D.; Avelino Corma, F.; © Luis, G. F. In *Studies in Surface Science and Catalysis*; Elsevier, 2000; Volume 130, pp 3303–3308.

(111) Ossipoff, N.; Cant, N. *Top. Catal.* **1999**, *8* (3), 161–169.

(112) Valden, M.; Pak, S.; Lai, X.; Goodman, D. W. *Catal. Letters* **1998**, *56* (1), 7–10.

(113) Haruta, M.; Tsubota, S.; Kobayashi, T.; Kageyama, H.; Genet, M. J.; Delmon, B. *J. Catal.* **1993**, *144* (1), 175–192.

(114) Zhu, G.; Qu, Z.; Zhuang, G.; Xie, Q.; Meng, Q.; Wang, J. *J. Phys. Chem. C* **2011**, *115* (30), 14806–14811.

(115) Brust, M.; Walker, M.; Bethell, D.; Schiffrin, D. J.; Whyman, R. *J. Chem. Soc. Chem. Commun.* **1994**, No. 7, 801–802.

(116) Xu, C.; Su, J.; Xu, X.; Liu, P.; Zhao, H.; Tian, F.; Ding, Y. *J. Am. Chem. Soc.* **2006**, *129* (1), 42–43.

(117) Zielasek, V.; Jürgens, B.; Schulz, C.; Biener, J.; Biener, M. M.; Hamza, A. V; Bäumer, M. *Angew. Chemie Int. Ed.* **2006**, *45* (48), 8241–8244.

(118) An, W.; Pei, Y.; Zeng, X. C. *Nano Lett.* **2007**, *8* (1), 195–202.

(119) Haruta, M. *ChemPhysChem* **2007**, *8* (13), 1911–1913.

(120) Enache, D. I.; Edwards, J. K.; Landon, P.; Solsona-Espriu, B.; Carley, A. F.; Herzing, A. A.; Watanabe, M.; Kiely, C. J.; Knight, D. W.; Hutchings, G. J. *Science (80-.).* **2006**, *311* (5759), 362–365.

(121) Takei, T.; Iguchi, N.; Haruta, M. *New J. Chem.* **2011**, *35* (10), 2227–2233.

(122) Karimi, B.; Esfahani, F. K. *Chem. Commun.* **2009**, No. 37, 5555–5557.

(123) Panten, J.; Surburg, H. In *Ullmann's Encyclopedia of Industrial Chemistry*; Wiley-VCH Verlag GmbH & Co. KGaA, 2000.

(124) Karimi, B.; Kabiri, E. F. *Chem. Commun.* **2009**, No. 37, 5555–5557.

(125) Kumar, S.; Zou, S. *Langmuir* **2007**, *23* (13), 7365–7371.

(126) Oros-Ruiz, S.; Pedraza-Avella, J.; Guzmán, C.; Quintana, M.; Moctezuma, E.; del Angel, G.; Gómez, R.; Pérez, E. *Top. Catal.* **2011**, 1–8.

(127) Lucchesi, C.; Inasaki, T.; Miyamura, H.; Matsubara, R.; Kobayashi, S. *Adv. Synth. Catal.* **2008**, *350* (13), 1996–2000.

(128) Templeton, A. C.; Chen, S.; Gross, S. M.; Murray, R. W. *Langmuir* **1999**, *15* (1), 66–76.

(129) Hostetler, M. J.; Green, S. J.; Stokes, J. J.; Murray, R. W. *J. Am. Chem. Soc.* **1996**, *118* (17), 4212–4213.

(130) Sugahara, K. N.; Teesalu, T.; Karmali, P. P.; Kotamraju, V. R.; Agemy, L.; Greenwald, D. R.; Ruoslahti, E. *Science (80-.).* **2010**, *328*, 1031–1035.

(131) Zako, T.; Nagata, H.; Terada, N.; Utsumi, A.; Sakono, M.; Yohda, M.; Ueda, H.; Soga, K.; Maeda, M. *Biochem. Biophys. Res. Commun.* **2009**, *381*, 54–58.

(132) Sugahara, K. N.; Teesalu, T.; Karmali, P. P.; Kotamraju, V. R.; Agemy, L.; Girard, O. M.; Hanahan, D.; Mattrey, R. F.; Ruoslahti, E. *Cancer Cell* **2009**, *16*, 510–520.

(133) Brauer, G. *Handbook of Preparative Inorganic Chemistry.*; 1965; Vol. 144.

(134) Ziegler, J.; Chang, R. T.; Wright, D. W. *J. Am. Chem. Soc.* **1999**, *121* (11), 2395–2400.

(135) Zhang, Y.; Terrill, R. H.; Tanzer, T. A.; Bohn, P. W. *J. Am. Chem. Soc.* **1998**, *120* (11), 2654–2655.

(136) Zhang, Y.; Terrill, R. H.; Bohn, P. W. *Chem. Mater.* **1999**, *11* (8), 2191–2198.

(137) Brewer, N. J.; Janusz, S.; Critchley, K.; Evans, S. D.; Leggett, G. J. *J. Phys. Chem. B* **2005**, *109* (22), 11247–11256.

(138) Sauerbrey, G. *Zeitschrift für Phys.* **1959**, *155* (2), 206–222.

(139) Janshoff, A.; Galla, H.-J.; Steinem, C. *Angew. Chemie Int. Ed.* **2000**, *39* (22), 4004–4032.